Continuous 25-years aerosol records at coastal Antarctica: Part 1. Inter-annual variability of ionic compounds and links to climate indices.

ROLF WELLER[1§*], DIETMAR WAGENBACH[2§], MICHEL LEGRAND[3], CHRISTOPH ELSÄSSER[2], XIANGSHAN TIAN-KUNZE[4], and GERT KÖNIG-LANGLO[1]

[1]Alfred Wegener Institute for Polar and Marine Research, Am Handelshafen 12, 27570 Bremerhaven, Germany,

[2]Institut für Umweltphysik, University of Heidelberg, Im Neuenheimer Feld 229, D-69120 Heidelberg, Germany,

[3]Laboratoire de Glaciologie et Géophysique de l'Environnement du Centre National de la Recherche Scientifique, St Martin d'Hères, France,

[4]Institut für Meereskunde, University of Hamburg, Bundesstraße 53, D-20146 Hamburg, Germany.

* Corresponding author: e-mail: Rolf.Weller@awi.de
§ Joint first authors

TeB-10-06-0035

Version 26.04.2011

Abstract

The aerosol climatology at the coastal Antarctic Neumayer Station (NM) was investigated based on continuous, 25 years long observations of biogenic sulfur components (methanesulfonate and non sea salt sulfate), sea salt and nitrate. Whilst significant long-term trends could only be detected for nitrate ($-3.6\pm2.5\%$ per year between 1983 and 1993 and $+4.0\pm3.2\%$ per year from 1993-2007), non-harmonic periodicities between 2 and 5 years were typical for all species. Dedicated time series analyses revealed that relations to sea ice extent and various circulation indices are weak at best or not significant. In particular, no consistent link between sea ice extent and sea salt loadings was evident suggesting only a rather local relevance of the NM sea salt record. Nevertheless, a higher Southern Annular Mode index tended to entail a lower biogenic sulfur signal. In examining the spatial uniformity of the NM findings we contrasted them to respective 17 years records from the coastal Dumont d'Urville Station (DDU). We found similar long term trends for nitrate, indicating an Antarctic-wide but not identifiable atmospheric signal, though any significant impact of solar activity or pollution could be ruled out. No inter-site variability on the multi annual scale was evident for the other ionic compounds.

1. Introduction

In addition to stable water isotopes recorded in Antarctic ice cores, important paleo-climate information comes from ionic impurities and insoluble dust preserved in this archive. In this context a review of the ionic ice composition originating from deposition of aerosol and water-soluble trace gases is given by Legrand and Mayewski, (1997). There is compelling evidence of large changes of mineral dust and sea salt entry to the Antarctic ice sheet over several climate cycles. At the same time little changes are seen for biogenic sulfur species and ammonium (Wolff et al., 2006; Kaufmann et al., 2010). In view of decadal to millennial scale variations during Holocene, ice core evidence on chemical change was less dramatic in accordance to the rather weak water isotope variability. Nevertheless, Mayewski et al. (2009) highlighted in a comprehensive review the pivotal role of chemical proxies in reconstructing the history of the Southern Ocean and Antarctic climate over the last few millennia. In this context, the most meaningful ionic impurities have proved to be the marine biogenic methanesulfonate (MS), non sea salt sulfate (nss-SO_4^{2-}) that is mainly biogenic or sporadically of volcanic origin, and Na^+, a genuine sea salt tracer. From Antarctic ice core records of these ions attempts were made to deduce the history of sea ice extent (Curran et al., 2003; Abram et al., 2007; Becagli et al., 2009), marine bio-productivity (Rhodes et al., 2009), as well as the southern atmospheric circulation pattern, including the Southern Annular Mode (SAM), Antarctic Dipole (ADP), Antarctic Circumpolar wave (ACW) and El Niño teleconnection (Fischer et al., 2004; Fundel et al., 2006; Mayewski et al., 2009). On the other hand, Russell and McGregor (2009) concluded that the paleo-atmospheric circulation reconstructions from ice core data appeared disturbingly inconsistent. Particularly the interpretation of nitrate records from Antarctic ice cores in terms of the governing atmospheric signal is still disputed. Unlike anthropogenic impact, which seems only evident in nitrate records from Greenland ice cores (Legrand and Mayewski, 1997; Fischer et al.,

1998), nitrate deposition onto the Antarctic ice sheet has been attributed to various sources including stratospheric N_2O oxidation and low latitude lightning activity (Legrand and Kirchner, 1990; Wolff, 1995), polar stratospheric cloud (PSC) precipitation (Mayewski and Legrand, 1990) and solar activity (e.g. McCracken et al., 2001; Palmer et al., 2001).

Evidently, in polar ice cores the signal of aerosol or reactive trace gas species depends on a large number of processes and parameters such as source strength, atmospheric chemistry, transport pattern, snow accumulation and post depositional processes, all being more or less climate related (particularly concerning the snow accumulation rate). In contrast, polar aerosol chemistry records are much less influenced by the precipitation variability. A possible link to climate signals should be more clearly detected in adequately long-term atmospheric observations of ionic species. However, such records exceeding one decade are rather sparse in Antarctica and only available from the coastal Antarctic stations NM (Wagenbach, 1996) or DDU (Jourdain and Legrand, 2002), while only relatively short and scattered atmospheric records are obtained so far at central Antarctic positions (Bodhaine et al., 1986; Harder et al., 2000; Weller and Wagenbach, 2007; Jourdain et al., 2008). The coastal aerosol chemistry records have already allowed detailed investigations of seasonal cycles, attribution of source regions as well as atmospheric transport and physico-chemical processes. Major findings of these studies indicate the almost exclusive marine biogenic source of atmospheric MS and nss-SO_4^{2-} governed by the productivity of the Southern Ocean (Minikin et al., 1998, Preunkert et al., 2008), sea ice as a significant sea salt source (Wagenbach et al., 1998a), and the association of Antarctic nitrate with the stratosphere (Mulvaney and Wolff, 1983; Wagenbach et al., 1998b; Weller et al., 2002; Savarino et al., 2007). In spite of this promising progress, (improving among others the interpretation of related signals in Antarctic ice cores) there exists no observational study specifically addressing the role of climate factors such as sea ice extent (SIE) or circulation patterns on the atmospheric variability of Antarctic chemical

aerosol species. Such an Antarctic aerosol climatology study requires appropriately long atmospheric observations like that provided by the Neumayer records presently covering more than 25 years.

Hence, we aim to investigate the long-term variability of the major ionic aerosol compounds MS, nss-SO_4^{2-}, NO_3^-, and Na^+ of the Neumayer data. Note that respective investigations of the seasonal cycles of these species has been reported elsewhere by Minikin et al. (1998), Wagenbach et al. (1998a and 1998b), Weller and Wagenbach (2007), and Weller et al. (2008). We report on the most abundant ionic species which are also the most widely used chemical proxies in Antarctic ice core studies. Unfortunately, mineral dust is not investigated here since the high aerosol sea salt loadings at NM prevented reliable determination of nss-Ca^{2+} and the longest record of crustal species is currently only 5 years (Weller et al., 2008), thus too short for a statistically significant mineral dust climatology. We evaluate the NM observations in the time and frequency (spectral) domain along with corresponding time series of SIE, SAM, and Southern Ocean Index (SOI) and contrast the results to a comparable 17 years long chemical aerosol record from DDU. Finally we discuss our atmospheric findings in view of the interpretation of glacio-chemical records, especially considering recent high resolution coastal ice core studies.

2. Experimental techniques and data evaluation methods

2.1. Site description, sampling and analytical procedures

For a detailed description of the NM sampling site, meteorological conditions, contamination free sampling, and analysis of the aerosol samples we refer to Wagenbach et al. (1988), König-Langlo et al. (1998) and Weller et al. (2008). In brief, a dedicated Air Chemistry Observatory was deployed in 1983 about 1.5 km south of the formerly Georg von

Neumayer station (70° 39' S, 8° 15'W; note that the station moves with the ice shelf around 160 m per year in northern direction towards the ice edge). The main catchment area of advected air masses relevant for the short lived atmospheric species was found to be the South Atlantic south of 50°S between 60°W and 30°E (Kottmeier and Fay, 1998; Reijmer and van den Brooke, 2000). Using an actively ventilated inlet stack, the air intake took place about 8 m above snow surface as to reduce the influence of drifting snow particles. From the in-line air stream aerosol was continuously sampled at 120 m^3 h^{-1} on two pre-cleaned Whatman 541 cellulose filters in series. The geometric settings upstream the filter face was designed as to commonly ensure sampling of particles with diameters of up to 10 μm, approximately. However, under high wind speed conditions particles that large may become already impacted at the sampling head orifice which would lead to a lower particle cut off.

   In 1991 the renewed observatory was relocated about 6 km south due to initial operation of the new Neumayer II Station (note that the abbreviation NM is uniformly used for both stations). Here we refer to samples taken from March 1983 through December 2007, comprising a temporal integration of 7 to 14 days (during the period 1983-1994 typically two weeks and 7 days thereafter) which corresponds to sample volumes of around 2_x10^4 m^3 to 4_x10^4 m^3 STP, respectively.

   As discussed by Weller et al. (2008) there were no significant sampling or contamination artefacts in the records, except some rare cases of filters wet by snow occurring during heavy blizzards. According to Wagenbach et al. (1998b) gaseous HNO$_3$ was collected as well due to the relative high sea salt loadings of the NM high volume filters. Thus the observed NO$_3^-$ data are assumed to be representative for total nitrate. This assessment was corroborated by low volume sampling during the years 2000 through 2007 using a teflon/nylon filter system, collecting all particulate compounds while around 90% of the gaseous HNO$_3$ is retained by the nylon filter (Piel et al., 2006). Comparison with our high volume filter sampling showed a

standard deviation of the total nitrate difference between both sampling methods of around ±48% and revealed no systematic trend or bias.

   All filter handling carried out in a class 100 laminar flow box in the field as well as in the home laboratories has been essentially identical through the years. The same holds true for extraction of the filter aliquots and subsequent ion chromatographic (IC) analyses performed from 1983 to 1994 at IUP (Wagenbach et al., 1988) and later on at AWI laboratories (Weller et al., 2008). The total errors were determined including the blank variability, the typical IC error (calibration error and baseline noise), and the error from the uncertainty of the sampled air volume. In short, the combined uncertainty was estimated between ±5% and ±11% for the components MS, NO_3^-, SO_4^{2-}, and Na^+ reported here. Non-sea salt sulfate (nss-SO_4^{2-}) concentrations were calculated by subtracting the concentration of the sea salt derived sulfate from the total SO_4^{2-} concentration (in ng g^{-1}). We used Na^+ as sea salt reference species and the sulfate to sodium ratio in bulk sea water of 0.252 during the November to February summer periods, while, following Wagenbach et al. (1998a), a ratio of 0.07 was used for winter (March through October) samples as accounting for the potential impact of sea salt fractionation during that season.

2.2. DDU aerosol records and auxiliary time series

   A comparable continuous long-term record of ionic aerosol composition started in 1991 at the French coastal Antarctic Station DDU (66°40'S, 140°01'E). The site and sampling procedures were described by Wolff et al. (1998). At this site, the aerosol sampling interval was typically 1-2 days, but could occasionally extend to 7 days in adverse weather conditions. In contrast to NM, Gelman Zefluor (PTFE, 47 mm diameter, 0.47 µm pore size) filters were used with air volume ranging from 70 m^3 up to 500 m^3. DDU is a site characterized by a high sea salt load in summer due to the proximity of open sea water (Wagenbach et al., 1998a) and

high ammonia levels related to the presence of a large penguin rockery (Legrand et al., 1998). Thus these abundant alkaline species make the observed NO_3^- data representative for total nitrate. The DDU data set will mainly be used to contrast our main NM findings with a coastal site differing in geographical and meteorological properties. Detailed comparison of NM and DDU aerosol records, which is beyond the scope of this paper are given by Wagenbach et al. (1998a and 1998b) and Minikin et al. (1998).

In order to identify possible links to Southern Ocean climate with the NM aerosol records we used the time series indices for SIE, SAM, and SOI backed up by the local meteorology including temperature, atmospheric pressure, and wind velocity. For these auxiliary records the same analyses in the time and spectral domain were performed. We emphasize that these analyses were restricted to the time period of the available aerosol measurements (1983-2007). Thus, the reported trends and oscillatory behavior of these auxiliary records may not reflect their climatology as a whole.

We refer to sea ice concentration data from National Snow and Ice Data Center (NSIDC, http://nsidc.org/) with a grid resolution of 25x25 km^2: From January 1983 to July 1987 Nimbus-7 Scanning Multichannel Microwave Radiometer (SMMR) data; from August 1987 to December 2007 Special Sensor Microwave/Imager (SSM/I) data. The data set has been generated using a bootstrap algorithm (Comiso, 1999). SIE was calculated with a longitudinal resolution of 10 degree. In each 10 degree sector the grid cells with at least 15% ice concentration were considered and the sum of the area was defined as the sea ice extent for the sector. The data were finally re-sampled to produce monthly mean SIE (i.e. sea ice area in units $10^6 \, km^2$). The accuracy of the retrieved SIE data is generally around ±5%, except during summer in regions where sea ice vanishes nearly completely. In the latter case the relative error can be as large as ±30% associated with a positive bias due to coastal spill over and atmospheric noise. One has to keep in mind that the uncertainty of the SIE during summer (up

to ±30%) could be within the range of its respective inter-annual variability making a meaningful correlation analysis in this case difficult. We focused our analysis on the region between 60°W and 30°E, based on the main marine source region of the advected air masses for NM. Due to the strong co-variance of the SIE between 60°W and 30°W as well as between 30°W and 30°E we combined the data in these longitude bins and restricted our evaluation primarily to these condensed entities. In case of DDU, the region between 90°E and 160°E has to be considered which was combined in an area between 90°E and 130°E and a second between 130°E and 160°E. According to Lemke et al. (2007) the over-all small positive trend observed in Antarctic SIE (1980-2005) is not statistically significant, in contrast to the strong decrease of sea ice coverage recently observed in the Arctic at the end of summer.

The SAM (also known as Antarctic Oscillation, AAO) is defined as the leading principal component (PC) of the 700 hPa geopotential height anomalies south of 20°S. The respective time series was retrieved from http://www.cpc.ncep.noaa.gov/products/precip/CWlink/ daily_ao_index/aao/aao_index.html. A recent evaluation based on reanalyses and observations stated a shift of SAM towards positive phase (lower pressure over Antarctica compared to southern mid-latitudes) during the 1958–2000 period, most pronounced since the late 1970s and coincident with a weakening of the semi-annual oscillation (SAO) (Marshall, 2003). In order to gauge the ENSO related variability we used the monthly Southern Ocean Index (SOI) (http://www.cdc.noaa.gov/data/climateindices/), which is defined as the twice–normalised difference in surface pressure between Tahiti and Darwin, Australia.

2.3. Time series analyses

Figure 1 shows an outline of the statistical data analyses accomplished in this study. The mathematical methods used for evaluation are described in the Supporting Information Appendix S1. Generally, all data records were analyzed in the time and frequency domain and trend estimates were based on the nonparametric rank-order Mann-Kendall test (Hirsch et al., 1982). Due to the fact that all methods employed for analyses in the spectral domain require a regular sampling time, adequate re-sampling of the multivariate data set was necessary. To this end, we averaged the signal over non-overlapping "bins" of equal time intervals τ of one month which results in an under-sampling of the time series, but avoided any data gaps and thus superseded interpolating procedures. Furthermore, normalised anomalies $X(\tau)$ for each running time step τ within the observation period were calculated as follows:

$$X(\tau) = [x(ij) - \langle x_i \rangle] / \sigma_i$$

Where $x(ij)$ is the mean of the measured parameter X for the month *i* for a given year *j*, $\langle x_i \rangle$ and σ_i are the mean and standard deviation over all years for this month. This procedure removes the seasonality and enables correlation and frequency analyses beyond the distinct seasonal cycle inherent to all records. The re-sampled data vectors $X(\tau)$ with $\tau = 1,\ldots,N$ and N = total number of months (i.e. the length of the time series), were also used to evaluate correlations among the measured parameters in the time domain.

The purpose of data evaluation in the frequency domain was to identify oscillatory patterns (harmonic as well as non-harmonic oscillations). Monte Carlo Singular Spectrum Analysis (MC-SSA) is particularly suited for extracting such information from short and noisy time series (e.g. Ghil et al., 2002). In short, MC-SSA comprises at first a decomposition of the time series in trend, oscillations, and noise components. These components are generated by data adaptive filters (eigenvectors), the so-called Empirical Orthogonal Functions (EOFs). EOFs

with the highest eigenvalues commonly represent the signal of the analysed time series, given that those eigenvalues are clearly separated from the remaining eigenvalues (e.g. Supporting Information Appendix 1, chapter S.1.3 and Appendix S3, Figs. S3.1 and S3.2). Finally, a reconstruction by a limited number of the calculated components potentially extracts signal from noise. In our case the sum of corresponding reconstructed components (RCs) showing periodicities >1 year were used to create a (noise-) filtered representation of the data which were further analysed by the Multitaper Method (MTM; Percival and Walden, (1993)). Compared to a direct spectral analysis of the original time series, this procedure enables a more straightforward interpretation of the results.

So far, these spectral methods provide only an estimate for significant frequencies (or periodicities) in a given time series $X(\tau)$, however, give no information on the coherence between common periodicities in different records. Phase locking, at least intermittently, indicates a potential causal link. Thus we calculated the magnitude-squared coherence (MSC) between two time series $X(\tau)$ and $Y(\tau)$ which is defined as the square of the cross-spectrum normalized by the individual power spectra, i.e. formally a correlation coefficient (with values between 0 and 1) in the frequency domain. However, this method provides no information on the temporal development of the coherence. Geophysical time series are rarely stationary in time, but contain intermittent periodicities. In order to detect intermittent (localized on the time axis) coherences in the time-frequency space, wavelet coherence transform (WCT) was used, based on an approach by Grinsted et al. (2004). Note that MSC and WCT actually detect only the coherence between two signals, but coherent frequencies do not necessarily have considerable power.

For all spectral methods employed here except MSC, we estimated the statistical significance against red noise, which is common in geophysical time series analyses. For MSC we used instead a nonparametric random phase estimate of significance according to

Ebisuzaki (1997) which is more stringent for this kind of correlation analysis. If not noted otherwise, we generally refer to $p = 0.05$ significance level.

3. Results

3.1. Data presentation

Figure 2 shows the 25-years long NM time series of the ionic aerosol compounds MS, nss-SO_4^{2-}, Na^+, and NO_3^- in monthly resolution (supplementary data are available at doi:10.1594/PANGAEA.756382), while in Fig. 3 corresponding diagrams for the anomalies are presented. In addition respecting figures of the DDU time series, the meteorological data from NM (temperature and wind speed) as well as SIE, SAM and SOI are shown in the Supporting Information Appendix S2 (Figs. S2.1 to S2.3). At both sites the concentration profiles of all compounds exhibit a distinct, non-stationary inter-annual variability. Generally, the standard deviations σ of the original data are roughly comparable to the corresponding annual means and particularly high for MS. Furthermore, concentration distributions were expectedly positively skewed for all ions, with mean/median ratios ranging from 1.26 (NO_3^-, NM) to 3.55 (MS, NM). Another common feature obvious in all NM ion records is the suspicious concentration minimum during the year 1993. A thorough inspection of the sampling conditions during this year did not indicate sampling artefacts or other peculiarities. Note that at both sites the sampling and analysing procedures were not changed during the whole observation period.

3.2. Analyses in the time domain

3.2.1. Impact of distinctive events and long-term trends. From Figs. 2 and 3 it is evident that none of the strong El Niño events consistently influenced the measured ion concentrations, at

NM. A trend analysis by the Mann-Kendall test with Sen's slope estimate revealed that the ion time series and their anomalies did not show a statistically significant trend within the time period of interest, except in case of nitrate at NM and DDU (Tab. 1). A closer look at the NM nitrate record (and derived anomalies) revealed a mean increase by 1.2±0.9% per year which include a decline over 1983-1993 of -3.6±2.5% per year followed by a 4.0±3.2% nitrate increase per year till the recent 2007 observations. Thereby, the strongest increase occurred within the period between 1993 and 2000 and subsequently levelled out (Figs. 2d and 3d).

Note that nss-SO_4^{2-} but definitely not MS decreased during last few years at DDU (Supporting Information Appendix S2, Fig. S2.1). At DDU, however, the nss-SO_4^{2-} calculation was confounded by the contamination from ornithogenic soils that contains significant amounts of both, sodium and sulfate (Jourdain and Legrand, 2002). Since the influence of respective inputs to the local boundary layer aerosol is not yet sufficiently settled, we do not further discuss the nss-SO_4^{2-} trend at DDU.

3.2.2. Correlations between ion records and climate parameters. In order to avoid spurious seasonality effects we first considered (normalized) monthly anomalies for this evaluation throughout. Correlation coefficients above the $p = 0.05$ significance level are listed in Tables 2 and 3 for NM and DDU, respectively. In general, even the most significant correlations of the ion records with SAM, SOI and SIE only describe less than 4% of the ion variability and are thus marginal. In a further attempt we correlated the corresponding annual mean values (where the use of anomalies is obsolete because all seasonal imprint is lost) of the ion records with the respecting climate parameters. This evaluation better reflects the situation for ice cores, where seasonal or even monthly resolution of the ionic profiles is rarely given. Furthermore, we considered the MS/nss-SO_4^{2-} ratio, which may be regarded as a crude proxy for the source region. High values point to more regional source regions south of 60°S,

although an interpretation of MS/nss-sulfate ratios is not straightforward (Legrand and Pasteur, 1998). To this end we rely on the mean MS/nss-SO_4^{2-} ratio for the month January each year which is representative for the summer maximum of biogenic sulfur aerosol. In addition also the annual means were used. The only correlations we found were those of the annual means record of nss-SO_4^{2-} and Na^+ with SIE 60°W-30°W (r = 0.42; p = 0.04) and with SOI (r = 0.45; p = 0.03), respectively (Table 2).

For the marine biogenic species MS and nss-SO_4^{2-} a considerable temporal lag between SIE, bio-productivity and finally atmospheric signal may be expected, reflecting the impact of winter SIE on phytoplankton bloom after retreat of the sea ice in spring (Curran et al., 2003; Abram et al., 2007). Nevertheless, at both sites monthly summer anomalies (Dec. through Feb.) showed no significant correlation of these ions, neither with the summer SIE anomalies (Dec. through Feb.) nor with the foregoing winter SIE anomalies (Jun. through Sep.). Due to the outstanding concentration maxima of MS and nss-SO_4^{2-} in mid-January each year, we also examined step by step the relation of the annual summer maxima of these ions with the mean SIE for January back to last July. In this case, at least for MS a significant correlation with the maximum SIE of the previous winter month August emerged with r = 0.46, p = 0.024 (see Table 2).

In conclusion, evaluation in the time domain revealed that the ionic aerosol records from NM and DDU exhibited a pronounced inter-annual variability, but long term trends and correlations with the climate related indices SIE, SAM, and SOI turned out to be only weak at best.

3.3. Analysis in the frequency domain

3.3.1. Characteristic periodicities. Even though correlations of ion records with climate factors appeared weak, a corresponding evaluation in the frequency domain may provide

additional information on links between ion records and climate, provided common periodicities and temporal coherency can be identified. In order to extract periodic signals from noise background, we performed a MC-SSA of the anomalies from all times series. The reconstructed compounds (see Supporting Information Appendix S3, Figs. S3.1 and S3.2) were examined by MTM frequency analysis. Tables 4 and 5 summarize the results of this evaluation step for the NM and DDU data, respectively. It emerged that frequencies <1/year found by MTM analyses were generally broadband, i.e. non-harmonic. Due to the chosen length of the embedded dimension (M = 60) of the MC-SSA, periodicities above about 5 years and below 1 year could not be further resolved in these reconstructed records. Obviously, periodicities in the range 2-5 years were characteristic for all ion records at NM as well as for SAM and SOI (Table 4). The MC-SSA indicated similar characteristic periodicities at DDU, although the results were not statistically robust, except for the leading EOFs of the ions nss-SO_4^{2-} and NO_3^- (Table 5). This may be due to the considerably shorter length of the time series from DDU. At least for NM, common periodicities between 2 and 5 years suggest a link between ion records and climate parameters SAM and SOI that is worth discussing.

3.3.2. Cross coherence behaviour. In a next step we examined the spectral coherencies between different time series by calculating the magnitude squared coherence (MSC) as well as wavelet coherence transform (WTC). Using the MSC and WCT analyses performed on the normalised anomalies $X(\tau_i)$ records, periodicities between 0.17 year (Nyquist frequency corresponding to one month sampling interval) and about 9 years and 12 years (≈1/2 the total length of the time series at DDU and NM) could in principle be resolved. It emerged that results from the correlation analyses appeared statistically not robust and often equivocal in the frequency (MSC) and time-frequency domain (WCT). Only in case where both methods showed statistically significant and consistent results the findings will be considered in the

later discussion (figures showing the results of the WCT analyses can be found in the Supporting Information Appendix S3). At NM, both spectral analytical tools showed formally meaningful results only for nss-SO_4^{2-} - SAM, nss-SO_4^{2-} - SIE 60°W-30°W as well as for local temperature versus nss-SO_4^{2-} and MS (Figs. 4-7). For the nss-SO_4^{2-} - SAM pair, MSC exhibited a peak at 4-6 years (Fig. 4), while WCT indicated a consistent phase locking at periodicities around 4 years located between 1989 and 1994 and also around 2-2.6 years between the years 2000 and 2004. Between nss-SO_4^{2-} and SIE 60°W-30°W, MSC showed a feature around 1.8 years (Fig. 5), consistent with WCT results. In the case of MS and nss-SO_4^{2-} versus temperature, broad significant coherences existed at periods of 2-3 years (Figs. 6 and 7). Concerning the shorter DDU observations, MSC and WTC indicated coherent periodicities (around 2 years and 4-6 years) only between NO_3^- and SAM (Supplementary Information Appendix S3, Fig. S3.7). In summary, except for nss-SO_4^{2-} versus temperature at NM, coherent periods were generally intermittent, i.e. not continuously present throughout the time domain. Thus, evaluations in the frequency domain supported the results already derived in the time domain. Overall, the represented variability of common periodicities appeared low in addition to weak coherencies between aerosol and climate related indices records (SIE, SAM, SOI) indicating a minor relevance of these couplings. It seems that the impact of Southern Ocean climate variability on the ionic composition of coastal aerosol is not unique and other processes determined the observed variability of the measured species.

4. Discussion

4.1. MS and nss-SO_4^{2-} time series.

   4.1.1. *Characteristics of Antarctic biogenic sulfur aerosol.* Previous evaluations of the long-term biogenic sulfur aerosol measurements at NM and DDU revealed that the main

source region for these sites is roughly located around 60°S (within the corresponding longitudinal sectors) with a more important MS contribution south of 60°S while a wider region north of 60°S is considered for nss-SO_4^{2-} (Minikin et al., 1998; Preunkert et al., 2007). A comparison of the annual mean MS data from NM and DDU displayed in Fig. 8 demonstrates the decoupled inter-annual variability indicating that source strength and transport pattern for biogenic sulfur are site specific. Note that different local meteorology at both sites may also influence near surface aerosol concentrations. While NM is more influenced by strong surface inversions but only by weak katabatic winds, the situation at DDU is vice versa (König-Langlo et al., 1998). A straightforward interpretation of biogenic sulfur signals in terms of climatic impact would involve the following aspects which are beyond the scope of the present paper: (i) the complex mechanisms controlling DMS emission from algae (Simó and Dachs, 2002; Simó, 2004), (ii) the subsequent complicated atmospheric chemistry of DMS oxidation (Yin et al., 1990; Jefferson et al., 1998; Preunkert et al., 2008; Read et al., 2008), and (iii) the overall different transport efficiency for MS and nss-SO_4^{2-} (Minikin et al., 1998; Piel et al., 2006; Preunkert et al., 2008).

4.1.2. Long term trends. An increasing trend in the atmospheric nss-SO_4^{2-} load from the 1950s onwards has been suggested from certain ice cores drilled in West Antarctica and thought to reflect the impact of anthropogenic sulfur emissions (Dixon et al., 2005). At least for the period 1983–2007 a comparable positive trend was clearly absent in our data at NM. Suggesting that for the past 25 years an anthropogenic impact on the sulfur budget of the Antarctic atmosphere is not substantiated by our records, the quoted ice core evidences should be reviewed in light of the atmospheric signal observed at NM.

4.1.3. Impact of SIE. There are several reasons to presume that SIE variations and climatic factors influencing SIE (e.g. the SAM) should significantly shape the long-term variability of atmospheric biogenic sulfur entry. Firstly, sea ice discharges micronutrients such as Fe during

melting (Sedwick and DiTullio, 1997) and secondly, lower winter temperatures provoke higher SIE and may cause higher biogenic production of the DMS precursor dimethylsulphoniopropionate (Stefels, 2000). However, there is a lack of observational evidence for a unique causal relation between SIE and DMS source strength. Considering the complex biochemical processes involved in phytoplankton derived DMS emissions (Stefels, 2000; Simó, 2004), such a definite relationship between both parameters can hardly be expected. Accordingly, at both sites MS and nss-SO_4^{2-} correlations with SIE in the time as well as frequency domain represented less than 4% of the sulfur signal variability and appeared ambiguous. However, the annual mean (but not maximum) nss-SO_4^{2-} and the maximum MS (but not the annual mean) concentrations emerged as stronger correlated with SIE 60°W-30°W (Table 2). Hence, on the whole the SIE - biogenic sulfur relations appeared somewhat inconsistent. Generally, at both sites the merely moderate departure of the SIE record from its long term mean was in contrast to the strong inter-annual variability of the biogenic sulfur signal (see respective annual means displayed in Fig. 9). From ice cores retrieved at coastal regions, positive (Pacific and Indic sector, Curran et al., 2003; Becagli et al., 2009) as well as negative (Atlantic sector, Abram et al., 2007) correlations with regional SIE have been deduced for MS. Nss-SO_4^{2-} profiles from West Antarctic ice cores appeared to be negatively correlated with SIE in the Amundsen-Ross Sea (Dixon et al., 2005). All these investigations referred to winter SIE, except Dixon et al. (2005) who correlated nss-SO_4^{2-} with the annually averaged SIE. Moreover, Rhodes et al. (2009) deduced from a snow pit at Mt. Erebus saddle a negative correlation between MS and summer SIE in the Ross Sea, which they explained by less extensive phytoplankton blooms during years with more extended summer sea ice. To our knowledge there exists no published ice core study evaluating MS in combination with nss-SO_4^{2-} in terms of SIE interaction. Neither from atmospheric (aerosol) nor from ice core studies a conclusive and unique mechanism in which way SIE might

influences biogenic sulfur emissions could be derived. It seems that the SIE – biogenic sulfur relationship is subtle and highly site specific and may be different for MS and nss-SO_4^{2-}.

4.1.4. Impact of SAM, SOI, and local temperature. The common periodicity of about 4 years detected in the MS, nss-SO_4^{2-}, SOI, and SAM time series (Table 4) is characteristic for the Southern Ocean quasi quadrennial oscillation and is also evident in the variance of the Antarctic Dipole (ADP) and the Antarctic Circumpolar Wave (ACW) (Yuan and Martinson, 2001; White and Peterson, 1996). The coherence found between nss-SO_4^{2-} and SAM at NM (Fig. 4) was located within this frequency range, but WCT indicated that the coherence was intermittent and the phase relation somewhat unclear and inconsistent (Supporting Information Appendix S3, Fig. S3.3). The reconstructed time series based on MC-SSA suggested that a higher SAM index, which typically corresponds to stronger development of the Antarctic vortex, intensified westerlies and less sea ice in the Weddell sector (Lefebvre et al., 2004; Thompson and Solomon, 2002), apparently provoked a lower biogenic sulfur signal in the atmosphere through the years 1987-2000 (Fig. 10). Nevertheless, even accepting that the 4 years periodicity in the biogenic sulfur signal may be entirely induced by the SAM, only about 17% of the MS or nss-SO_4^{2-} variability could be represented in this way (Table 4).

The striking positive correlation of biogenic sulfur with local temperature at NM in the time and frequency domain remains peculiar. As a plausible explanation we suggest that warmer summer temperatures provoked an earlier retreat of local sea ice, especially in the nearby Atka Bay, entailing enhanced local marine bio-productivity. In conclusion, only the correlation between biogenic sulfur and local temperature at NM was consistent in the time and the frequency domain, indicating that local to regional effects in concert with the aerosol transport may control the long-term variability of these aerosol components. Also recent ice core studies from the Weddell Sea region (Abram et al., 2007) suggested that atmospheric transport is a decisive factor for the biogenic sulfur entry into this region.

4.2. Na$^+$ (sea salt) time series.

 4.2.1. Characteristics of Antarctic sea salt aerosol. On a global scale, the dominant mechanism producing sea salt aerosol is bubble bursting during whitecap formation caused by surface winds over open ocean waters (Monahan et al., 1986). For Polar Regions, the formation of sea salt aerosols on freshly formed sea ice (via frost flowers; Rankin et al. (2002), Wolff et al. (2003)) or snow on sea ice (Yang et al., 2008) is being considered as alternative or even dominant source. This assumption challenging the interpretation that sea salt signals in ice cores should be a proxy for storminess and meridional transport proposed by Petit et al. (1999). Actually, there is further evidence from aerosol measurements in continental Antarctica for fractionated sea salt entry, i.e. sea salt with markedly depleted ss-SO$_4^{2-}$ contingent (Jourdain et al., 2008) pointing to a sea ice source. SIE should play a crucial, but counteracting role in both potential sea salt generation mechanisms: In the traditional case (bubble bursting) the area of the interface open water – atmosphere is decisive which decreases with increasing SIE, while in the second case (freshly formed) sea ice itself is the source. Both processes should certainly benefit from high wind velocities, albeit the micro-physical processes mobilising sea salt aerosol from sea ice or frost flowers still remains to be clarified. Note that respective time series assessing the area of freshly formed sea ice (being a potential sea salt aerosol) are not available. We assume that this freshly formed sea ice roughly correlated with total SIE.

 4.2.2. Impact of local meteorological parameters. The negative correlation between Na$^+$ signal and local atmospheric pressure anomalies (Table 2) suggests that low pressure systems (associated with higher storminess) promoted the sea salt aerosol entry at NM. Indeed, storminess and wind velocity exhibits a broad maximum during the winter months at NM though a close link between local wind velocity and Na$^+$ concentrations could not be verified

(Weller et al., 2008). A recent model study by Korhonen et al. (2010) concluded that the decadal increases in Southern Hemisphere (50°S-65°S) wind speeds since the early 1980s caused a higher sea spray flux, implying an increasing sea salt aerosol trend at coastal sites which, however, was not seen, neither at NM nor at DDU.

4.2.3. Impact of SIE. Apparently in contradiction to the recently proposed frost flower source (Rankin et al. (2002), Wolff et al. (2003)), we found a very marginal anti-correlation between SIE and sea salt aerosol entry at NM and DDU and a significant (positive) correlation with local temperature at NM (Tables 2 and 3). In a further approach we investigated at both sites the correlation between Na^+ and SIE for winter (May through October) and summer (November through March) separately, with the seasonal windows selected by the occurrence of seawater-SO_4^{2-} depletion following Wagenbach et al. (1998a). In all cases slightly negative, but statistically not significant correlations (r between -0.1 and -0.23; p >0.2) were detected. The higher inter-annual variability of the Na^+ signal compared to SIE (Fig. 9) was another conspicuous feature already found for biogenic sulfur compounds, and indicating that sea salt load changes in the boundary layer air in coastal Antarctica was not controlled by the regional SIE.

4.2.4. Relation to atmospheric circulation indices. Interestingly, a prominent >5 years periodicity (Tab. 4) was evident in the Na^+ record at NM, close to the 7 years cycle frequently identified in ice cores from the plateau region of Dronning Maud Land (Fischer et al., 2004). This 7 years periodicity may actually be ascribed to the variability of the Amundsen Sea Low (ASL), but was only noticeable between 1965 and 1990 in ice cores from the Weddell Sea region (Kreutz et al., 2000). A strengthening of the ASL usually results in high pressure over the Weddell Sea and South Atlantic, entailing low SIE in this region. Nevertheless, our analyses revealed no significant spectral coherence between sea salt concentration anomalies and SIE in the Weddell Sea region (60°W-30°W) within this periodicity range.

On the other hand an outstanding feature of our measured Na$^+$ aerosol record at NM was a distinct minimum in 1993 (Figs. 2c and 3c), coinciding with an elongated phase of high SAM index. A comparison of the MC-SSA filtered time series (see Supporting Information Appendix S3, Figs. S3.1 and S3.2) as well as all correlation analyses indicated that this potential link was probably fortuitous and does not persist within the entire observational period.

We may conclude that a unique relation between atmospheric Na$^+$ concentrations and SIE or the climatology of atmospheric circulation indices (represented by SAM and SOI) was not obvious at both sites. Instead, the varying influence of the potential sea salt aerosol sources which depends critically on surface wind velocity and the efficiency of atmospheric transport to the sampling site appeared to be more decisive. Note that similar to MS, also Na$^+$ showed a decoupled inter-annual variability between NM and DDU (Fig. 8).

4.2.5. Site specific aspects. In contrast to other ionic species, sea salt aerosol measurements at coastal stations are potentially biased by local effects due to the largely varying proximity of the open water or sea ice sources (Wagenbach et al., 1998a). The contribution of very locally generated sea salt aerosol, however, was mitigated since supra micron particles (broadly above 7-10 µm, constituting a significant fraction of the local sea salt load) were not efficiently sampled due to the cut-off properties of our air inlet, designed to discriminate against drifting ice crystals. Even so, local factors may have blurred the possible long-term variability impact of SIE or circulation patterns on the sea salt aerosol changes at NM. Furthermore, sea salt aerosol load over continental Antarctica is about an order of magnitude lower compared to coastal sites while the corresponding gradient for biogenic sulfur is much less distinct (Weller and Wagenbach, 2007), although the primary source region for both aerosol compounds is the interface ocean - atmospheric boundary layer. In case of sea salt variability, the inconclusive and missing relation to large scale driving processes was most

likely due to the overwhelmingly local influences on this signal. Hence, based on our results meaningful implications on the interpretation of respective ice core records cannot be given.

4.3. Nitrate time series.

4.3.1. Characteristics of Antarctic nitrate aerosol. Evaluation of NM records of total nitrate, $\delta^{15}N(NO_3^-)$ (Wagenbach et al., 1998b), and gaseous reactive nitrogen oxides (NO$_y$; Weller et al., 2002) already indicated that the multi-modal, seasonal input above background of these N-compounds is mainly associated with stratospheric sources. This finding, including nitrate from sedimentation of polar stratospheric clouds (PSC) in late winter to early summer and late summer stratospheric air mass intrusions was refined by combining $\delta^{15}N$, $\delta^{18}O$, and $\Delta^{17}O$ analyses in atmospheric nitrate (Savarino et al., 2007). Their detailed year-round analyses made for the coastal site of DDU point to HNO_3 evaporated directly from the snow and/or HNO_3 formed by oxidation of NO_x emitted from the snow after photolysis of nitric acid in the snowpack. This recycled nitrate substantially accounted for the multi-modal nitrate peak, but the respective contribution of these two processes to the atmospheric nitric acid level remains unclear (see Davis et al. (2008) for a review). Possibly, evaporation is the dominant process at sites with very low snow accumulation rates (Röthlisberger et al., 2002; Weller et al., 2004), but not elsewhere where photolysis becomes the dominant process even at inland sites like the South Pole (Arimoto et al., 2008). Accordingly, our present time series analyses of the de-seasonalized anomalies, may not capture these processes which manifest themselves in the multi-modal seasonal nitrate peak shape.

Interestingly, the significant post 1993 nitrate variability and associated enhancement was also observed at DDU (Fig. 11) providing an inter-site correlation of the annual mean nitrate levels around r = 0.68 (Fig. 8). In discussing the causes for the striking inter-annual nitrate variability and trend, we may consider: (i) filter sampling artefacts arising from a

systematically changing sea salt level, (ii) stratospheric NO_y variability driven by long term growing N_2O emissions and/or large scale hemispheric circulation changes, (iii) polar stratospheric NO_y variability driven by proton precipitation (galactic cosmic rays and/or solar proton events) depending on the solar activity, (iv) strengthening of the polar vortex and polar stratospheric clouds (PSC) sedimentation, (v) growing anthropogenic NO_x emissions from mid southern latitudes and/or from Antarctic station activities, (vi) changes in the snow recycling of nitric acid.

4.3.2. Filter sampling artefacts due to changing sea salt load. As discussed by Wagenbach et al. (1998b), it cannot be excluded that during summer the high level of acidic sulfur aerosol and lower sea-salt load caused a loss of HNO_3 by remobilization of nitrate collected on the filter. As seen in Figs. 2c and 2d, before 1995 there was a common pattern between the long term sea salt and nitrate records at NM, which was mainly governed by the absolute annual minimum in 1993 but also a decreasing trend from 1983 to 1993. This minimum, which for unknown reasons was a common feature to all displayed ion species and particularly distinct for nitrate and sea salt (see also illustrations of anomalies in Fig. 3) did not manifest in the aerosol-borne [7]Be and ^{210}Pb radionuclide species (Elsässer et al., 2011). However, after the 1993 minimum, the shape of the Na^+ anomaly record was barely reflected in the NO_3^- anomaly record (Figure 3). Furthermore, the increase of nitrate from 1993 to 2007 at NM was also evident at DDU. Also corroborated by parallel total nitrate measurements we can exclude that the trend and variability of atmospheric nitrate at NM and DDU were driven by a changing HNO_3 collection efficiency.

4.3.3. Impact of growing N_2O emissions and stratospheric NO_y source. The major primary source of stratospheric NO_y is nitrous oxide (N_2O) whose levels have recently grown at a rate of 0.26% per year (Forster et al., 2007) with a greater increase of stratospheric NO_2 (5% per decade from 1980 to 1998) reported by Liley et al. (2000) from Lauder in New-Zealand

(45°S). These differing trends were explained by a simultaneous change of the NO_y/NO_2 partitioning resulting from the decreasing ozone and increasing halogen trends (McLinden et al., 2001). Consequently, we cannot expect a straightforward relation between the trends of N_2O and one of its stratospheric oxidation products.

The study of the variability and trend of stratospheric NO_2 conducted by Cook and Roscoe (2009) in Antarctica indicated that in high southern latitude regions another important factor is the strength of the Brewer-Dobson circulation which conveys tropospheric N_2O into the tropical stratosphere and from there toward the winter pole. A weakened Brewer-Dobson circulation would permit a more complete oxidation of N_2O into reactive nitrogen in the tropical stratosphere. Discarding the years 1991 and 1992 during which the Pinatubo volcanic cloud had disturbed the NO_y partitioning (see further discussions below), the long-term NO_2 vertical column observed in Antarctica by Cook and Roscoe (2009) revealed a broad maximum around 2000. This maximum may be caused by a weakened Brewer-Dobson circulation close to the solar maximum and coincides with a strong negative Quasi Biennial Oscillation (QBO). Nevertheless, Cook and Roscoe (2009) concluded that much of the increase from 1990 to 2000 remained unexplained. Considering the broad maximum in the surface nitrate records at DDU and NM around 2000, a decisive difference to the stratospheric load of NO_2 was the absence of a distinct further decrease in the surface nitrate records, otherwise clearly obvious in the NO_2 column after 2000 (Cook and Roscoe, 2009).

Slusser et al. (1997) and Cook and Roscoe (2009) attributed the marked reduction of the NO_2 stratospheric load seen between 1991 and 1992 to the impact of the eruption plume of Mt. Pinatubo (entailing an efficient hydrolysis of N_2O_5 and $BrONO_2$ on volcanogenic sulfuric acid aerosol to HNO_3 resulting in a net NO_2 depletion). However, the shift of the NO_y partitioning in the stratosphere in favour of nitric acid during the volcanic period was not detected in the surface nitrate record. This absence of enhanced nitrate surface levels would

suggest a more limited downward transport of nitrate during this period. Finally, it is not obvious how these processes could result in the one year delayed surface nitrate minimum observed at NM and DDU in 1993.

4.3.4. Impact of proton precipitation over Antarctica. Galactic cosmic rays (GCR, energetic proton precipitation) are a source of NO through dissociative ionization of N_2 in the lower stratosphere particularly at high latitudes (Nicolet, 1975). The resulting NO production varies in opposite phase with the solar activity cycle. The missing coherence of nitrate with the 11 years modulation of the GCR flux clearly present in the cosmogenic Be-isotopes at NM (Elsässer et al., 2011) makes it unlikely that the cosmic ray variability along with solar activity mediated NO production had substantially driven the long term nitrate change. This conclusion is consistent with the fact that the NO production from cosmic rays remains weak compared to the N_2O oxidation contribution, even at the polar tropopause (10% versus 90%, Legrand et al., 1989). As is expected, neither an imprint of outstanding solar proton events (SPE) over the observation period like that of 1989, nor their clustering (broadly during solar minima) in the periods 1989-1994 and 2001-2006 appeared to be reflected in the long term inter-annual nitrate variability (see Figs. 2d and 3d).

4.3.5. Impact of PSC sedimentation and strength of the polar vortex. Intensification of the stratospheric Antarctic ozone hole since the early 1980s, decreasing stratospheric temperatures (Randel et al., 2009), strength of the polar vortex, and increasing PSC occurrence are interlinked (Solomon, 1999), although PSC mediated nitrate deposition may not respond in a direct way to increasing spring ozone depletion. The outstanding weak ozone depletion events in the years 1988 and 2002 certainly associated with less PSC occurrence were not reflected in the observed nitrate record at NM, indicating only a minor correlation of PSC occurrence on the coastal surface nitrate variability. One would expect that the strength of the polar vortex affects both, the efficiency of stratosphere-troposphere exchange,

subsiding stratospheric derived nitrate, and also the development and persistency of katabatic winds which potentially carry HNO_3 enriched boundary layer air from continental Antarctica to coastal sites. The positive correlation with the SAM index (and with the SOI, influencing SAM), suggested a significant but minor net impact of the variability of the polar vortex strength on the nitrate budget at NM and DDU.

4.3.6. Anthropogenic impact. On first sight, growing anthropogenic emissions in Antarctica during the last 25 years (Shirsat and Graf, 2009; Graf et al., 2010) and steadily increasing NO_x emissions in the Southern Hemisphere (Lelieveld et al., 2004) may potentially be reflected in long term nitrate observations at Antarctic sites. If we confine the issue to the seasonal background nitrate prevailing from April through June (and carrying the $\delta^{15}N$ signature characteristic for the remote troposphere; Wagenbach et al., 1998b, Savarino et al., 2007), a significant increasing trend of 0.32 ng yr^{-1} i.e. 1.9% per year referring to the mean background nitrate level of 17 ng m^{-3} was obvious at NM. Almost identical increase rates were seen at DDU with 0.25 ng yr^{-1} i.e. 1.98% per year referring to the mean background nitrate concentration of 12.6 ng m^{-3}. One may speculate if this background nitrate, being less influenced by re-emitted or stratospheric nitrate (Wagenbach et al., 1998b) might reflect a potential increase of anthropogenic nitrate emissions in the Southern Hemisphere as a whole. Nevertheless, the shape of the long term nitrate change at NM appeared inconsistent with a potential steadily growing anthropogenic source. Also no significant black carbon trend (continuously recorded at NM since 1999; Weller, unpublished results) could be detected. Thus, the role of anthropogenic emissions on the NM long term nitrate change was not evident, especially not in view of the declining nitrate trend leading to the grand minimum around 1993 and the virtually constant level 2000 onwards (Figs. 2d and 3d).

4.3.7. Recycling of deposited nitrate. Whatever the source, nitrate, once deposited in the snow, can either be directly re-emitted as volatile HNO_3 (Röthlisberger et al., 2002; Weller et

al., 2004) or photochemically converted into gaseous NO_x (see review by Grannas et al., 2007 and references therein) and may significantly contribute to the summer nitrate peak at coastal sites (Savarino et al., 2007; Frey et al., 2009). Enhanced short-wave UV radiation during springtime ozone depletion should foster photochemical NO_x release from the snow surface (Weller et al., 2002; Frey et al., 2009). Intensification of the stratospheric Antarctic ozone hole began in the early 1980s, although the positive trend in the NM nitrate record was not evident before 1993 (Figs. 2d and 3d) and as mentioned before, outstanding weak ozone depletion events of the years 1988 and 2002 were not reflected therein. These findings indicate an only minor influence of photochemically induced nitrate recycling (as mediated by the ozone hole changes) on the inter-annual variability in the observed nitrate time series. The relevance of re-emitted nitrate, simply caused by evaporation of HNO_3 from acidic summer firn layers (Röthlisberger et al., 2002), however, cannot be assessed from our results. Finally, we note that changing sea salt deposition in nitrate-remobilisation regions could significantly change firn acidity and thus the impact of this process.

4.3.8. Summary of nitrate findings. Keeping in mind the rather weak, though nominally significant long term nitrate trend at NM (echoed in the overlapping period since 1991 by the atmospheric nitrate observations at DDU), we could not attribute a definite cause for those observations. It should also be noted that long-term mean nitrate concentrations at DDU were about 25% lower compared to NM. One may speculate whether the fact that DDU was more often outside the polar vortex than NM entails less PSC precipitation and less photochemical recycling of once deposited nitrate during the ozone hole period. It is noteworthy that the long term trend as well as the inter-annual variability of nitrate since 1992 was the only signal clearly common to both NM and DDU sites and thus was driven by an Antarctic wide forcing mechanism. Apart from the rather intricate source mix, made up by direct (PSC sedimentation, stratospheric air mass intrusion) and indirect (nitrate mobilisation from inland

surface firn) processes, also long term sea salt deposition changing at the re-mobilisation region might have contributed. Importantly, none of the solar effects known to influence the NO_y production on various time scales, particularly in the polar middle atmosphere were significantly reflected in the 25 years atmosphere surface nitrate record.

Considering Antarctic firn or ice cores at the whole and even disregarding net nitrate loss, we are confronted with weak temporal resolution, remaining dating error, indispensable post depositional smoothing, and a sea salt dependent total deposition velocity. Thus, in view of the failure to attribute clear causes even to the observed atmospheric nitrate record it is unlikely that ice core nitrate concentrations alone (e.g. without additional isotopic evidence) may hold the history of stratospheric chemistry and dynamics or solar activity changes. The latter finding is supported by recent snow and firn investigations reported by Wolff et al. (2008) from the coastal Halley Station.

5. Concluding Remarks

Spanning more than 25 years, the continuous atmospheric observation of ionic aerosol species at the coastal Antarctic Neumayer Station constitutes the longest of such records within the Antarctic realm. In view of this extended observational period we attempted to establish a coastal Antarctic aerosol climatology focussing on the long term and inter-annual variability of major ion components comprising biogenic sulfur (MS and nss-SO_4^{2-}), sea salt, and nitrate. Dedicated time series analyses in the time and frequency domains revealed no statistically significant trends except for nitrate which decreased over the 1983-1993 period and increased thereafter. The actual cause for the observed nitrate trends could not be assigned but we suppose that a combination of dynamical and photochemical processes associated with ozone changes in the Antarctic stratosphere might have played a significant

role in this phenomenon. In any case, we may preclude here the impact of solar activity (including solar proton events) or anthropogenic pollution.

Examinations of the generally marked inter-annual aerosol changes for possible links in the time as well as frequency domain with climate related indices (including SIE, SOI, SAM, and local meteorological parameters) showed weak correlations at best, which were mostly inconsistent and barely meaningful on that time scale. Although periodicities in the range of 2-5 years were found to be typical for all four NM records as well as for SAM, SOI and broadly SIE indices, the represented variability of common periodicities were marginal making the imprint of climate related parameters on the aerosol records irrelevant.

A lack of long term variability observed in the NM aerosol records was generally confirmed by DDU which showed no notable coherence with the NM records except for a quite similar long term nitrate increase. Confirmation of the observed inter-annual NO_3^- variability at other sites would be needed to proof that this finding is an Antarctic-wide signal. Comparable to NM only very marginal links to the climate related indices could be detected in the respective time series from DDU suggesting that: (i) the nitrate long term change was most probably driven by an Antarctic wide signal and, (ii) the atmospheric biogenic sulfur and sea salt variability was dependent on a patchy oceanic source distribution and on regional scale transport patterns and was not spatially uniform within the coastal Antarctic realm.

Overall, these findings, valid for both coastal sites, appear to contradict results from various glacio-chemical ice core studies performed in marine influenced Antarctic areas. Strictly speaking, based on atmospheric observations the link between aerosol signals and SIE or mean atmospheric circulation pattern was not that evident as suggested by current interpretations of ice core derived decadal changes of biogenic sulfur and sea salt species (see e.g. Curran et al., 2003; Dixon et al. 2005; Rhodes et al., 2009).

In commenting this apparent discrepancy we first address possible shortcomings inherent to the atmospheric NM records: In view of the extremely high sea salt variability at this site owing, among others, to its proximity to the open water and sea ice related source, the weak response of the locally relevant sea salt signal to the variability of SIE and circulation indices is not surprising. However, this drawback is less evident for the biological sulfur species and nitrate for which atmospheric changes are less influenced by fluctuating sources. Although West Antarctica and especially the Antarctic Peninsula experienced a unique warming in recent decades (Monaghan et al., 2008; Steig et al., 2009), SAM and particularly SIE did not show a pronounced trend or outstanding changes during the observational NM period. This specific situation may not necessarily be the case for the much longer time scale accessible in ice cores studies. Finally, we have to bear in mind that sites where a relationship between ionic ice core records and SIE was apparently successful are located distant from the Antarctic coast. Dedicated long-term atmospheric measurements on chemical composition of the aerosol from ice core drilling sites are obviously needed, but such investigations have not been initiated until recently (Jourdain et al., 2008).

In contrast to the atmospheric observations, ion records from Antarctic firn cores are commonly associated with a relatively weak temporal resolution, significant dating errors, various post depositional smoothing processes or even re-mobilisation in case of nitrate and MS. One would expect, therefore, that the changes seen in the atmospheric records are not so distinctly recorded in related ice core sections. Moreover, the most important ice core drawback concerns the fact, that they may not directly report atmospheric concentrations, but only respective changes which are mediated by the related snow accumulation rate. Obviously all the above mentioned ice core shortcomings are to a different extent connected to the snow accumulation rate which in turn is sensitive to climate properties (ranging from synoptic weather pattern to long term changes, see e.g. Bromwich, 1988 and Noone et al., 1999).

Focusing on the latter point, it is evident that the ion variability in ice cores depends not only on the respective accumulation quantity but also on the (least known) timing of precipitation within the seasonal cycle of the atmospheric load. This effect is expected to be particularly critical for biogenic sulfur species and nitrate for which extreme seasonal amplitudes are seen in the atmospheric records. Generally, stacking of several ice core profiles might remove or at least alleviate such depositional noise.

Taking the main findings of the long term variability in our atmospheric records we argue that a good deal of climate related links apparently contained in glacio-chemical records of Antarctic ice core might be mediated by the accumulation variability and, therefore, not seen in the corresponding atmospheric records. Combining the time resolution and direct recording advantage of the atmospheric records with the longer time scale and the (noise reducing) higher spatial coverage of ice cores may help to substantiate this question. Ironically, nitrate the only species where a clear temporal signal stands out in the atmospheric records, may be least reliably recorded in Antarctic ice cores unless the accumulation is high enough to prevent post depositional nitrate changes.

References

Abram, N.J., Mulvaney, R., Wolff, E.W., and Mudelsee, M. 2007. Ice core records as sea ice proxies: An evaluation from the Weddell Sea region of Antarctica. *J. Geophys. Res.* **112**, D15101, doi:10.1029/2006JD008139.

Arimoto, R., Zeng, T., Davis, D., Wang, Y., Khaing, H., Nesbit, C., and Huey, G. 2008. Concentrations and sources of aerosol ions and trace elements during ANTCI-2003. *Atmos. Environ.* **42**, 2864-2876, doi:10.1016/j.atmosenv.2007.05.054.

Becagli, S., Castellano, E., Cerri, O., Curran, M, Frezzotti, M., and co-authors. 2009. Methanesulphonic acid (MS) stratigraphy from a Talos Dome ice core as a tool in depicting sea ice changes and southern atmospheric circulation over the previous 140 years. *Atmos. Environ.* **43**, 1051-1058.

Bodhaine, B.A., Deluisi, J.J., Harris, J.M., Houmere, P. and Bauman S. 1986. Aerosol measurements at the South Pole. *Tellus* **38***B*, 223-235.

Bromwich, D.H. 1988. Snowfall in High Southern Latitudes. *Rev. Geophys.* **26**(1), 149-168.

Comiso, J. 1999. Bootstrap sea ice concentrations from NIMBUS-7 SMMR and DMSP SSM/I (01 January 1983 to 31 December 2007), National Snow and Ice Data Center, Digital media, Boulder, CO.

Cook, P.A. and Roscoe, H.K. 2009. Variability and trends in stratospheric NO_2 in Antarctic summer, and implications for stratospheric NO_y. *Atmos. Chem. Phys.* **9**, 3601-3612.

Curran, M.A.J., van Ommen, T.D., Morgan, V.I., Phillips, K.L., Palmer, A.S. 2003. Ice Core Evidence for Antarctic Sea Ice Decline since the 1950s. *Science* **302**, 1203-1206.

Davis, D.D., Seelig, J., Huey, G., Crawford, J., Chen, G., and co-authors. 2008. A reassessment of Antarctic plateau reactive nitrogen based on ANTCI 2003 airborne and ground based measurements. *Atmos. Environ.* **42**, 2831-2848, doi:10.1016/j.atmosenv.2007.07.039.

Dixon, D., Mayewski, P.A., Kaspari, S., Kreutz, K., Hamilton, G., Maasch, K., Sneed, S.B., and Handley, M.J. 2005. A 200 year sulfate record from 16 Antarctic ice cores and associations with Southern Ocean sea-ice extent. *Ann. Glaciol.* **41**, 155-166.

Ebisuzaki, W. 1997. A method to estimate the statistical significance of a correlation when the data are serially correlated. *J. Clim.* **10**, 2147-2153.

Elsässer, C., Wagenbach, D, Weller, R., Auer, M., Wallner, A., and Christl, M. 2011. Continuous 25-years aerosol records at coastal Antarctica: Part II. Variability of the radionuclides ^{7}Be, ^{10}Be and ^{210}Pb. *Tellus 63B*, this issue.

Fischer, H., Wagenbach, D., and Kipfstuhl, J. 1998. Sulfate and nitrate firn concentrations on the Greenland ice sheet 1. Large-scale geographical deposition changes. *J. Geophys. Res.* **103**(D17), 21,927-21,934.

Fischer, H., Traufetter, F., Oerter, H., Weller, R., and Miller, H. 2004. Prevalence of the Antarctic Circumpolar Wave over the last two millenia recorded in Dronning Maud Land ice. *Geophys. Res. Lett.* **31**, L08202, doi:10.1029/2003GL019186.

Forster, P., Ramaswamy, V., Artaxo, P., Berntsen, T, Betts, and co-authors. 2007. Changes in Atmospheric Constituents and Radiative Forcing. In: *Climate Change 2007: The Physical Science Basis*. Contribution *of Working Group I to the Fourth Assessment Report of the Intergovernmental Panel on Climate Change* [Solomon, S., D. Qin, M. Manning, Z. Chen, M. Marquis, K.B. Averyt, M. Tignor and H.L. Miller (eds.)], pp. 143-145. Cambridge University Press, Cambridge, United Kingdom and New York, NY, USA.

Frey, M.M., Savarino, J., Morin, S., Erbland, J., and Martins, J.M.F. 2009. Photolysis imprint in the nitrate stable isotope signal in snow and atmosphere of East Antarctica and implications for reactive nitrogen cycling. *Atmos. Chem. Phys.* **9**, 8681-8696.

Fundel, F., Fischer, H., Weller, R., Traufetter, F., Oerter, H., and Miller, H. 2006. Influence of large-scale teleconnection patterns on methane sulfonate ice core records in Dronning Maud Land. *J. Geophys. Res.* **111**, D04103, doi:10.1029/2005JD005872.

Ghil, M., Allen, M.R., Dettinger, D., Die, K., Kondrashov, D., and co-authors. 2002. Advanced spectral methods for climatic time series. *Rev. Geophys.* **40**, 1-41, doi:10.1029/2001RG000092.

Graf, H.-F., Shirsat, S.V., Oppenheimer, C., Jarvis, M.J., Podzun, R., and Jacob, D. 2010. Continental scale Antarctic deposition of sulfur and black carbon from anthropogenic and volcanic sources. *Atmos. Chem. Phys.* **10**, 2457-2465.

Grannas, A.M., Jones, A.E., Dibb, J., Ammann, M., Anastasio, C. and co-authors. 2007. An overview of snow photochemistry: evidence, mechanisms and impacts. *Atmos. Chem. Phys.* **7**, 4329-4373.

Grinsted, A., Moore, J.C., and Jevrejeva, S. 2004. Application of the cross wavelet transform and wavelet coherence to geophysical time series. *Nonlinear Processes in Geophysics* **11**, 561-566.

Harder, S., Warren, S.G. and Charlson, R.J. 2000. Sulfate in air and snow at the South Pole: Implications for transport and deposition at sites with low snow accumulation. *J. Geophys. Res.* **105**(D18), 22 825-22 832.

Hirsch, R.M., Slack, J.R., and Smith, R.A. 1982. Techniques of trend analysis for monthly water quality data. *Water Resour. Res.* **18**, 107-121.

Jefferson, A., Tanner, D.J., Eisele, F.L., Davis, D.D., Chen, G., Crawford, J., Huey, J.W., Torres, A.L., and Berresheim H. 1998. OH photochemistry and methane sulfonic acid formation in the coastal Antarctic boundary layer. *J. Geophys. Res.*, *103*(D1)*, 1647-1656.

Jourdain, B. and Legrand M. 2002. Year-round records of bulk and size-segregated aerosol composition and HCl and HNO_3 levels in the Dumont d'Urville (coastal Antarctica)

atmosphere: Implications for sea-salt aerosol fractionation in the winter and summer. *J. Geophys. Res.* **107**(D22)*,* 4645, doi:10.1029/2002JD002471.

Jourdain, B., Preunkert, S., Cerri, O., Castebrunet, H., Udisti, R., and Legrand, M. 2008. Year-round record of size-segregated aerosol composition in central Antarctica (Concordia station): Implications for the degree of fractionation of sea-salt particles. *J. Geophys. Res.* **113**, D14308, doi:10.1029/2007JD009584.

Kaufmann, P., Fundel, F., Fischer, H., Bigler, M., Ruth, U., and co-authors. 2010. Ammonium and non-sea-salt sulfate in the EPICA ice cores as indicator of biological activity in the Southern Ocean. *Quaternary Science Reviews* **29**, 313-323 doi:10.1016/j.quascirev.2009.11.009.

König-Langlo, G., King, J.C., Pettré, P. 1998. Climatology of the three coastal Antarctic stations Dumont d'Urville, Neumayer and Halley. *J. Geophys. Res.* **103**(D9)*,* 10 935-10 946.

Korhonen, H., Carslaw, K.S., Forster, P.M., Mikkonen, S., Gordon, N.D., and Kokkola, H. 2010. Aerosol climate feedback due to decadal increases in Southern Hemisphere wind speeds. *Geophys. Res. Lett.* **37**, L02805, doi:10.1029/2009GL041320.

Kottmeier, C. and Fay, B. 1998. Trajectories in the Antarctic lower troposphere. *J. Geophys. Res.* **103,** 10 947-10 959.

Kreutz, K.J., Mayewski, P.A., Pittalwala, I.I., Meeker, L.D., Twickler, M.S., and Whitlow, S.I.. 2000. Sea level pressure variability in the Amundsen Sea region inferred from a West Antarctic glaciochemical record. *J. Geophys. Res.* **105**(D3), 4047-4059.

Lefebvre, W., Goosse, H., Timmermann, R., Fichefet, T. 2004. Influence of the Southern Annular Mode on the sea ice-ocean system. *J. Geophys. Res.* **109**, C09005, doi:10.1029/2004JC002403.

Legrand, M., Stordal, F., Isaksen, I.A., and Rognerud, B. 1989. A model study of the stratospheric budget of odd nitrogen, including effects of solar cycle variations. *Tellus* **41B**, 413-426.

Legrand, M. and Kirchner, S. 1990. Origins and variations of nitrate in South Polar precipitation. *J. Geophys. Res.* **95**(D4), 3493-3507.

Legrand, M. and Mayewski, P. 1997. Glaciochemistry of polar ice cores: a review. *Rev. Geophys.* **35**, 219-243.

Legrand, M. and Pasteur, E.C. 1998. Methane sulfonic acid to non-sea salt sulfate ratio in coastal Antarctic aerosol and surface snow. *J. Geophys. Res.* **103**(D9)*,* 10 991-11 006.

Legrand, M. Ducroz, F., Wagenbach, D., Mulvaney, R., and Hall, J. 1998. Ammonium in coastal Antarctic aerosol and snow: Role of polar ocean and penguin emissions. *J. Geophys. Res.* **103**(D9), 11,043-11,056.

Lelieveld, J., van Aardenne, J., Fischer, H., de Reus, M., Williams, J., and Winkler, P. 2004. Increasing Ozone over the Atlantic Ocean. *Science* **304**, 1483-1487.

Lemke, P., Ren, J., Alley, R.B., Allison, I., Carrasco, J., Flato, G., Fujii, Y., Kaser, K., Mote, P., Thomas, R.H., and Zhang, T. 2007. Observations: Changes in Snow, Ice and Frozen Ground. In: *Climate Change 2007: The Physical Science Basis. Contribution of Working Group I to the Fourth Assessment Report of the Intergovernmental Panel on Climate Change* [Solomon, S., D. Qin, M. Manning, Z. Chen, M. Marquis, K.B. Averyt, M. Tignor and H.L. Miller (eds.)], pp 350-355. Cambridge University Press, Cambridge, United Kingdom and New York, NY, USA.

Liley, J.B., Johnson, P.V., McKenzie, R.L, Thomas, A.L., and Boyd, I.S. 2000. Stratospheric NO_2 variations from long time series at Lauder, New Zealand. *J. Geophys. Res.,* **105**, 11,633-11,640.

Marshall, G.J. 2003. Trends in the Southern Annular Mode from Observations and Reanalyses. *J. Climate* **16**, 4134-4143.

Mayewski, P.A. and Legrand, M. 1990. Recent increase in nitrate concentration of Antarctic snow. *Nature* **346**, 258-260.

Mayewski, P.A., Meredith, M.P., Summerhayes, C.P., Turner, J., Worby, A., and co-authors. 2009. State of the Antarctic and southern ocean climate system. *Rev. Geophys.* **47**, RG1003, 1-38, doi:10.1029/2007RG000231.213

McCracken, K.G., Dreschhoff, G.A.M., Zeller, E.J., Smart, D.F., and Shea, M.A. 2001. Solar cosmic ray events for the period 1561-1994 1. Identification in polar ice, 1561-1950. *J. Geophys. Res.* **106**(A10), 21,585-21,598.

McLinden, C.A., Olsen, S.C., Prather, M.J., and Liley, J.B. 2001. Understanding trends in stratospheric NO_y and NO_2. *J. Geophys. Res.* **106**, 27,787-27,793.

Minikin, A., Legrand, M., Hall, J., Wagenbach, D., Kleefeld, C., Wolff, E., Pasteur, E.C. and Ducroz, F. 1998. Sulfur-containing species (sulfate and methanesulfonate) in coastal Antarctic aerosol and precipitation. *J. Geophys. Res.* **103**(D9), 10 975-10 990.

Monaghan, A.J., Bromwich, D.H., Chapman, W., and Cosimo, J.C. 2008. Recent variability and trends of Antarctic near-surface temperature. *J. Geophys. Res.* **113**, D04105, doi:10.1029/2007JD009094.

Monahan, E.C., Spiel, D.E. and Davidson, K.L. 1986. A model of marine aerosol generation via whitecaps and wave disruption. In: *Oceanic Whitecaps* (ed. E. Monahan and G.M. Niocaill). D. Reidel, Norwell, Mass., 167-174.

Mulvaney, R. and Wolff, E.W. 1993. Evidence for Winter/Spring Denitrification of the Stratosphere in the Nitrate Record of Antarctic Firn Cores. *J. Geophys. Res.* **98**(D3), 5213-5220.

Nicolet, M. 1975. On the production of nitric oxide by cosmic rays in the mesosphere and stratosphere. *Planet. Space Sci.* **23**, 637-649.

Noone, D., Turner, J., and Mulvaney, R. 1999. Atmospheric signals and characteristics of accumulation in Dronning Maud Land, Antarctica. *J. Geophys. Res.* **104**(D16), 19,191-19,211.

Palmer, A.S., van Ommen, T.D., Curran, M.A.J., and Morgan, V. 2001. Ice-core evidence for a small solar-source of atmospheric nitrate. *Geophys. Res. Lett.* **28**(10), 1953-1956.

Percival, D.B., and Walden, A.T. 1993. *Spectral Analysis for Physical Applications.* Cambridge Univ. Press, New York, 583 pp.

Petit, J.R., Jouzel, J., Raynaud, D., Barkov, N.I., Barnola, J.-M., and co-authors. 1999. Climate and atmospheric history of the past 420,000 years from the Vostok ice core, Antarctica. *Nature* **399**, 429-436.

Piel, C., Weller, R., Huke, M. and Wagenbach, D. 2006. Atmospheric methane sulfonate and non-sea salt sulfate records at the EPICA deep-drilling site in Dronning Maud Land, Antarctica. *J. Geophys. Res.* **111**(D03304), doi:10.1029/2005JD006213.

Preunkert, S., Legrand, M., Jourdain, B., Moulin, C., Belviso, S., Kasamatsu, N., Fukuchi, M., and Hirawake, T. 2007. Interannual variability of dimethylsulfide in air and seawater and its atmospheric oxidation by-products (methanesulfonate and sulfate) at Dumont d'Urville, coastal Antarctica (1999-2003). *J. Geophys. Res.* **112**, D06306, doi:10.1029/2006JD0075857.

Preunkert, S., Jourdain, B., Legrand, M., Udisti, R., Becagli, S., and Cerri, O. 2008. Seasonality of sulfur species (dimethyl sulphide, sulfate, and methanesulfonate) in Antartica: Inland versus coastal regions. *J. Geophys. Res.* **113**, D15302, doi:10.1029/2008JD009937.

Randel, W.J., Shine, K.P., Austin, J., Barnett, J., Claud, C., and co-authors. 2009. An update of observed stratospheric temperature trends. *J. Geophys. Res.* **114**, D02107, doi:10.1029/2008JD010421.

Rankin, A.M., Wolff, E.W. and Martin, S. 2002. Frost flowers: Implications for tropospheric chemistry and ice core interpretation. *J. Geophys. Res.* **107**(D23), 4683, doi:10.10129/2002JD002492.

Read, K.A., Lewis, A.C., Bauguitte, S., Rankin, A.M., Salmon, R.A., and co-authors. 2008. DMS and MS measurements in the Antarctic Boundary Layer: impact of BrO and MS production. *Atmos. Chem. Phys.* **8**, 2985-2997.

Reijmer, C.H., and van den Brooke, M.R. 2000. Moisture sources of precipitation in Western Dronning Maud Land, Antarctica. *Antarct. Sci.* **13**(2), 210-220.

Rhodes, R.H., Bertler, N.A.N., Baker, J.A., Sneed, S.B., Oerter, H., and Arrigo, K.R. 2009. Sea ice variability and primary productivity in the Ross Sea, Antarctica, from methylsulphonate and snow record. *Geophys. Res. Lett.* **36**, L10704, doi:10.1029/2009GL037311.

Röthlisberger, R., Hutterli, M.A., Wolff, E.W., Mulvaney, R., Fischer, H., and co-authors. 2002. Nitrate in Greenland and Antarctic ice cores: a detailed description of post-depositional processes. *Annals of Glaciology*, **35,** 209-216.

Russel, A., and McGregor, G.R. 2009. Southern hemisphere atmospheric circulation: impacts on Antarctic climate and reconstructions from Antarctic ice core data. *Climatic Change*, doi:10.1007/s10584-009-9673-4.

Savarino, J., Kaiser, J., Morin, S., Sigman, D.M., and Thiemens, M.H. 2007. Nitrogen and oxygen isotopic constraints on the origin of atmospheric nitrate in coastal Antarctica. *Atmos. Chem. Phys.* **7**, 1925-1945.

Sedwick, P.N. and DiTullio, G.R. 1997. Regulation of algal blooms in Antarctic shelf waters by the release of iron from melting sea ice. *Geophys. Res. Lett.* **24**(20), 2515-2518.

Shirsat, S.V. and Graf, H.F. 2009. An emission inventory of sulfur from anthropogenic sources in Antarctica. *Atmos. Chem. Phys.* **9**, 3397-3408.

Simó, R. and Dachs, J. 2002. Global ocean emission of dimethylsulfide predicted from biogeophysical data. *Global Biochem. Cycles,* **16**(4), 1078, doi:10.1029/2001GB001829.

Simó, R. 2004. From cells to globe: approaching the dynamics of DMS(P) in the ocean at multiple scales. *Can. J. Fish. Aquat. Sci.* **61**, 673-684.

Slusser, J.R., Fish, D.J., Strong, E.K., Jones, R.L., Roscoe, H.K., and Sarkissian, A. 1997. Five years of NO_2 vertical column measurements at Faraday (65°S): Evidence for hydrolysis of $BrONO_2$ on Pinatubo aerosols. *J. Geophys. Res.* **102**(D11), 12,987-12,993.

Solomon, S. 1999. Stratospheric ozone depletion: A review of concepts and history. *Rev. Geophys.* **37**, 275-316.

Stefels, J. 2000. Physiological aspects of the production and conversion of DMSP in marine algae and higher plants. J. Sea Res. 43, 183-197, doi:10.1016/S1385-1101(00)00030-7.

Steig, E.J., Schneider, D.P., Rutherford, S.D., Mann, M.E., Cosimo, J.C., and Shindell, D.T. 2009. Warming of the Antarctic ice-sheet surface since the 1957 International Geophysical Year. Nature 457, 459-463, doi:10.1038/nature07669.

Thompson, D.W.J., and Solomon, S. 2002. Interpretation of recent southern Hemisphere climate change. *Nature* **296**, 895-899.

Wagenbach, D., Görlach, U., Moser, K., and Münnich, K.O. 1988. Coastal Antarctic aerosol: the seasonal pattern of its chemical composition and radionuclide content. *Tellus* **40B**, 423-436.

Wagenbach, D. 1996. Coastal Antarctica: Atmospheric chemical composition and atmospheric transport. In: *Chemical Exchange between the Atmosphere and polar snow* (ed.

E.W. Wolff and R.C. Bales). NATO ASI Series vol. **43***, Springer-Verlag Berlin Heidelberg, 173-199.

Wagenbach, D., Ducroz, F., Mulvaney, R., Keck, L. Minikin, A., Legrand, M., Hall, J.S. and Wolff, E.W. 1998a. Sea salt aerosol in coastal Antarctic regions. *J. Geophys. Res.* **103**(D9), 10,961-10,974.

Wagenbach, D., Legrand, M., Fischer, H., Pichlmayer, F. and Wolff, E.W. 1998b. Atmospheric near-surface nitrate at coastal Antarctic sites. *J. Geophys. Res.* **103**(D9)*, 11,007-11,020.

Weller, R., Jones, A.E., Wille, A., Jacobi, H.-W., McIntyre, H.P., Sturges, W.T., Huke, M., Wagenbach, D. 2002. Seasonality of reactive nitrogen oxides (NO_y) at Neumayer Station, Antarctica. *J. Geophys. Res.* **107**(D23), 4673, doi:10.1029/2002JD002495.

Weller, R., Traufetter, F., Fischer, H., Oerter, H., Piel, C. and Miller, H. 2004. Post depositional losses of methane sulfonate, nitrate and chloride at the EPICA deep-drilling site in Dronning Maud Land, Antarctica. *J. Geophys. Res.* **109**(D07301), doi:10.1029/2003/JD004189.

Weller, R. and Wagenbach, D. 2007. Year-round chemical aerosol records in continental Antarctica obtained by automatic samplings. *Tellus* **59B**, 755-765, doi:10.111/j.1600-0889.2007.00293.x

Weller, R., Wöltjen, J., Piel, C., Resenberg, R., Wagenbach, D., König-Langlo, G., and Kriews, M. 2008. Seasonal variability of crustal and marine trace elements in the aerosol at Neumayer station, Antarctica. *Tellus* **60B**, 742-752, doi:10.111/j.1600-0889.2008.00272.x

White, W.B. and Peterson, R.G. 1996. An Antarctic circumpolar wave in surface pressure, wind, temperature and sea-ice extent. Nature 380, 699-702.

Wolff, E.W.. 1995. Nitrate in polar ice. In: *Ice Core Studies of Global Biogeochemical Cycles* (ed. R. Delmas). NATO ASI Series Vol. **30***, Springer-Verlag Berlin Heidelberg, 193-240.

Wolff, E.W., Legrand, M., Wagenbach, D. 1998. Coastal Antarctic aerosol and snowfall chemistry. *J. Geophys. Res.* **103**(D9), 10,927-10,934.

Wolff, E.W., Rankin, A.M., and Röthlisberger, R. 2003. An ice core indicator of Antarctic sea ice production. *Geophys. Res. Lett.* **30**(22)*,* 2158, doi:10.1029/2003GL018454.

Wolff, E.W., Fischer, H., Fundel, F., Ruth, U., Twarloh, B., and co-authors. 2006. Southern Ocean sea-ice extent, productivity and iron flux over the past eight glacial cycles. *Nature* **440***,* 491-496, doi:10.1038/nature04614.

Wolff, E.W., Jones, A.E., Bauguitte, S. J.-B., and Salmon, R.A. 2008. The interpretation of spikes and trends in concentration of nitrate in polar ice cores, based on evidence from snow and atmospheric measurements. *Atmos. Chem. Phys.* **8**, 5627-5634.

Yang, X., Pyle, J.A., and Cox, R.A. 2008. Sea salt aerosol production and bromine release: Role of snow on sea ice. *Geophys. Res. Lett.* **35**, L16815, doi:10.1029/2008GL034536.

Yin, F., Grosjean, D., Flagan, R.C., and Seinfeld, J.H. 1990, Photooxidation of dimethyl sulfide and dimethyl disulfide: Mechanisms evaluation, *J. Atmos. Chem,* **11**, 365-399.

Yuan, X. and Martinson, D.G. 2001. The Antarctic Dipole and its predictability. *Geophys. Res. Lett.* **28**(18), 3609-3612.

Supporting Information

Additional supporting information may be found in the online version of this article:

Appendix S1 Short description of the methods used for time series analyses

Appendix S2 Presentation of ancillary time series

Appendix S3 Ancillary results regarding spectral coherence

Table 1. Significant long term linear trends detected in the ionic records from NM and DDU.

component	site	observed period	trend
NO_3^-	NM	1983-2007	$+0.51$ ng yr^{-1} $+1.2$ % yr^{-1}
NO_3^-	NM	1991-2007	$+1.46$ ng yr^{-1} $+3.4$ % yr^{-1}
NO_3^-	DDU	1991-2007	$+0.78$ ng yr^{-1} $+2.5$ % yr^{-1}

Table 2. Correlation coefficients (r) between ionic compounds measured at NM and climate parameters. Results are based on monthly anomalies, except entries in parentheses. Only correlations significant above a $p = 0.05$ significance level are listed.

component (anomaly)	SIE 60°W-30°W	SIE 30°W-30°E	SOI	SAM	temperature	pressure
MS	$(0.46)^a$		0.133		0.133	
nss-SO_4^{2-}	$(0.42)^b$				0.205	
NO_3^-			0.178	0.132	-0.136	
Na^+		-0.115	$(0.45)^b$		0.16	-0.131

[a] January value of MS correlated with SIE 60°W-30°W maximum of the forgoing winter/spring
[b] Based on annual mean values

Table 3. Same as Table 2 but for Dummont D'Urville

component (anomaly)	SIE 90°E-130°E	SIE 130°E-160°E	SOI
nss-SO_4^{2-}		-0.191	-0.196
NO_3^-		0.147	0.143
Na^+	-0.219		

Table 4. Results of the MC-SSA for the NM records: analyzed component (anomaly), EOFs showing long periodicities, detected periodicity of the corresponding reconstructed components (generally non-harmonic) based on the listed EOFs, and represented variance. Diagrams of the respecting reconstructions as well as the eigenvalue spectra can be found in the Supporting Information Appendix S3, Figs. S3.1 and S3.2).

component (anomaly)	EOF [number]	period [yr]	explained variance
MS	1+2	4.2	9.0%+8.3%
nss-SO_4^{2-}	1+2	4.2	8.9%+8.1%
NO_3^-	1	>5	27%
	2*	(>5)	(8.1%)
	3*+4*	(3)	(3.9%+3.6%)
Na^+	1	>5	11.5%
	2	≈5	5.4%
sea ice 60°W-30°W	1+2	>5	9.2%+7.4%
	3*	(3)	(4.3%)
sea ice 30°W-30°E	1*+2*	(>5)	(14.4%+9.9%)
SAM	1*+2	≈5	5.2%+4.9%
	3+4	2.1	4.5%+4.4%
SOI	1*+2	≈5	14.1%+13.2%
	3+4	3.3	9.7%+9.1%

* according to MC-SSA not significant on at p = 0.05 significance level

Table 5. Results of the MC-SSA for the DDU records. Note that none of the EOF were significantly above red noise level, except the EOF 1 for nss-SO_4^{2-} and NO_3^- reflecting the trend of these records.

component (anomaly)	EOF [number]	period [yr]	explained variance
MS	1*+2*	(1.3)	(6.2%+5.8%)
nss-SO_4^{2-}	1	-	22.8%
	3*+4*	(2-3)	(3.5%+3.1%)
NO_3^-	1	-	14.8%
	2*+3*	(1.6)	(7.2%+7.0%)
	3*+4*	(4.2)	(6.1%+5.4%)
Na^+	-	-	-
sea ice 90°E – 130°E	1*	(>5)	(12.2%)
	2*+3*	(4-5)	(9.5%+7.0%)
sea ice 130°E – 160°E	1*+2*	(2)	(12.3%+11.4%)

[*] according to MC-SSA not significant at $p = 0.05$ significance level
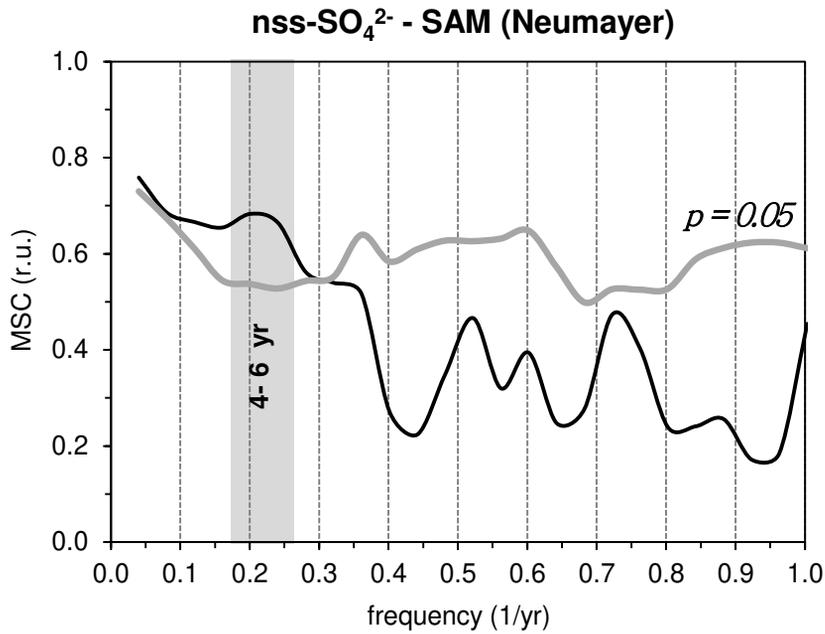
Figure captions.

Fig. 1. Outline of the performed data analyses; MTM = Multiple Taper Method, MC-SSA = Monte Carlo Singular Spectrum Analysis. In addition correlations in the time domain were also calculated using corresponding annual mean values of all parameters.

Fig. 2. Monthly mean concentrations of ionic aerosol components observed at NM: (a) MS; (b) $nss\text{-}SO_4^{2-}$; (c) Na^+; (d) NO_3^-. Grey vertical bars mark distinct El Niño events (1982, 1986, 1997, and 2006).

Fig. 3. Same as Fig.2 but for monthly mean anomaly time series.
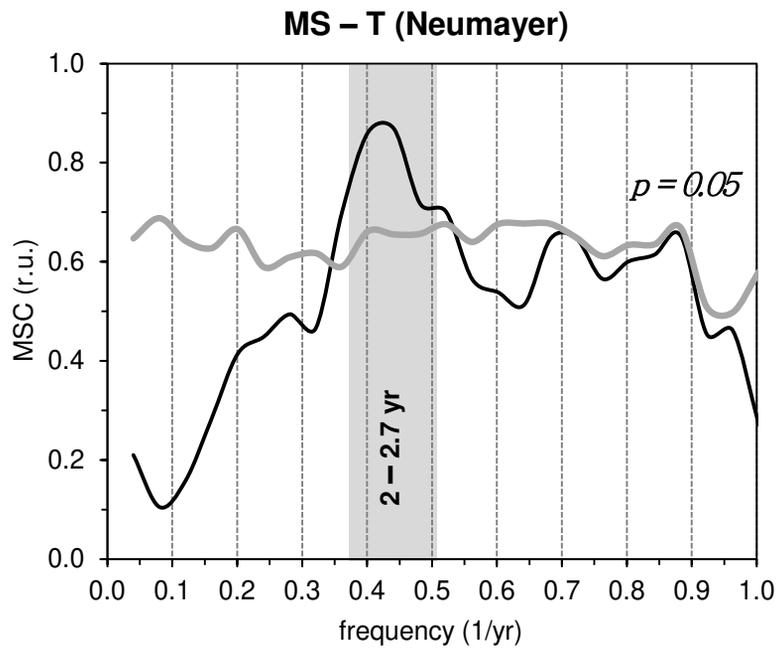
Fig. 4. Magnitude squared coherence between the NM $(nss\text{-}SO_4^{2-})_{anomaly}$ and the SAM (bold black line; grey line: p = 0.05 significance level). Only the frequency range $< 1\ yr^{-1}$ is shown and lines are smoothed by cubic spline fits.
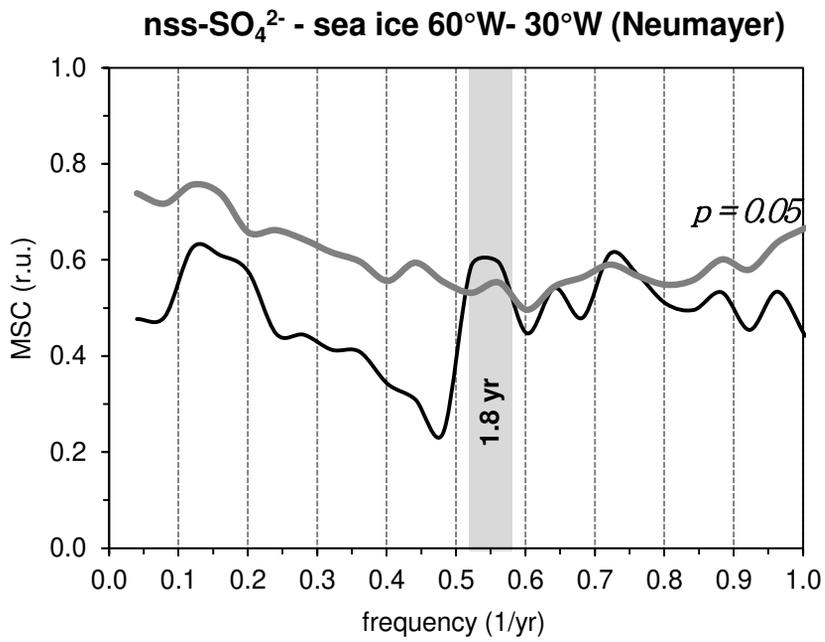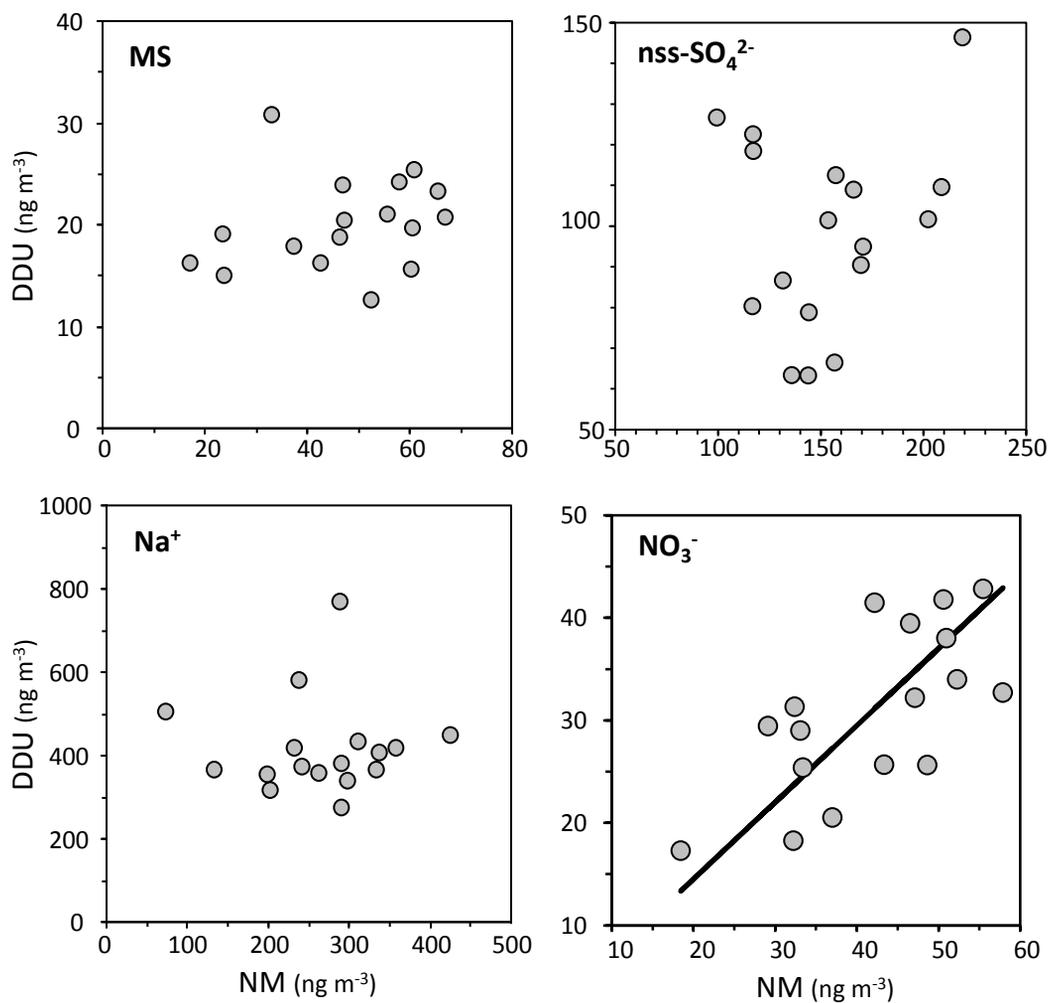
Fig. 5. Magnitude squared coherence between the NM $(nss\text{-}SO_4^{2-})_{anomaly}$ and the SIE at 60°W-30°W (bold black line; grey line: p = 0.05 significance level).
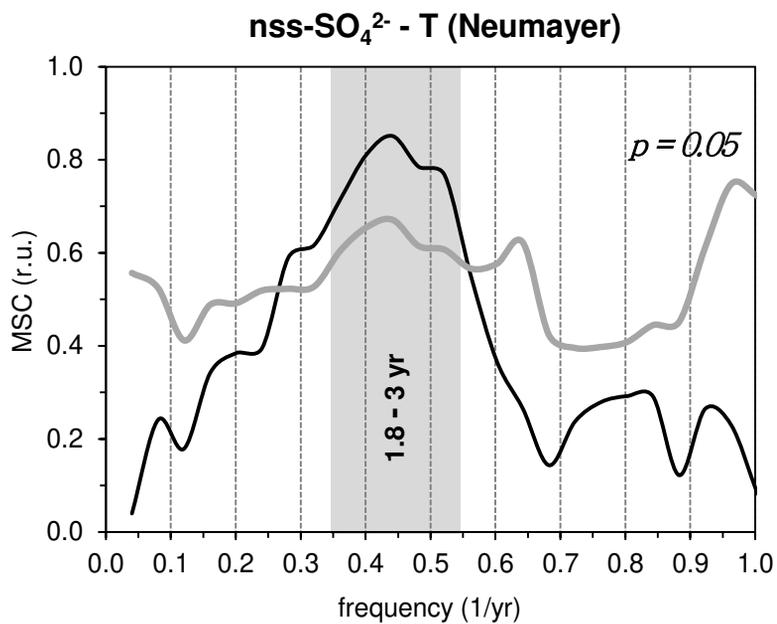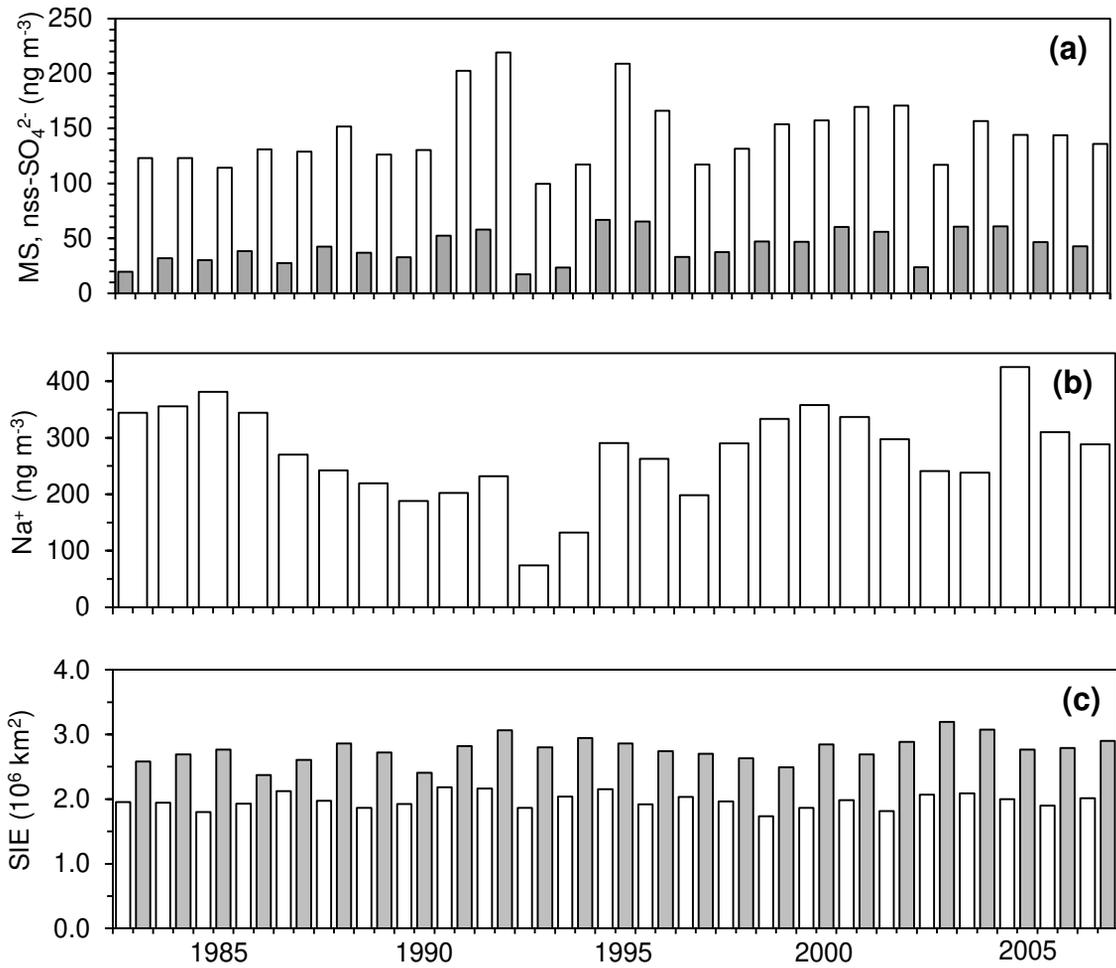
Fig. 6. Magnitude squared coherence between the NM $(nss\text{-}SO_4^{2-})_{anomaly}$ and local temperature T, (bold black line; grey line: p = 0.05 significance level).
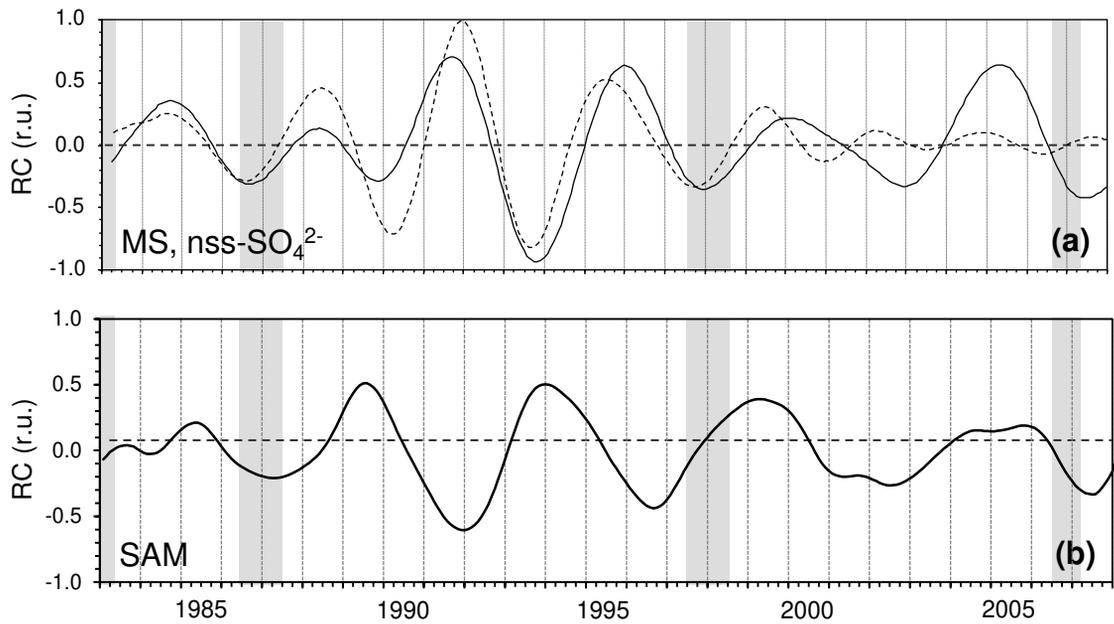
Fig. 7. Magnitude squared coherence between the NM $(MS)_{anomaly}$ and local temperature T, (bold black line; grey line: p = 0.05 significance level)

Fig. 8. Scatter plots of annual mean ion concentrations measured at NM (abscissa) and DDU (ordinate), respectively. The regression line for NO_3^- is based on a bivariate reduced major axis (RMA) regression: y = 0.75($\pm$0.16) $-$ 0.5($\pm$6), r^2 = 0.47.

Fig. 9. Annual means of: (a) MS (grey bars) and nss-SO_4^{2-} (white bars), (b) Na^+, all at NM, (c) SIE 60°W-30°W (white bars) and SIE 30°W-30°E (grey bars).

Fig. 10. Results from the Monte Carlo Singular Spectrum Analyses (MC-SSA). Plotted are the sum of corresponding RCs showing periodicities larger than one year: (a) MS (solid line) and nss-SO_4^{2-} (dashed line) anomaly reconstructions according to EOF 1+2 each. (b) SAM reconstruction according to EOF 1+2. Grey vertical bars mark El Niño events.

Fig. 11. Comparison of the monthly mean NO_3^- record observed Neumayer (lower panel) and DDU (upper panel).

Fig. 1. Outline of the performed data analyses; MTM = Multiple Taper Method, MC-SSA = Monte Carlo Singular Spectrum Analysis. In addition correlations in the time domain were also calculated using corresponding annual mean values of all parameters.

Fig. 2. Monthly mean concentrations of ionic aerosol components observed at NM: (a) MS; (b) nss-SO_4^{2-}; (c) Na^+; (d) NO_3^-. Grey vertical bars mark distinct El Niño events (1982, 1986, 1997, and 2006).

Fig. 3. Same as Fig.2 but for monthly mean anomaly time series.

nss-SO₄²⁻ - SAM (Neumayer)

Fig. 4. Magnitude squared coherence (MSC) between the NM $(nss-SO_4^{2-})_{anomaly}$ and the SAM (bold black line; grey line: $p = 0.05$ significance level). Only the frequency range < 1 yr^{-1} is shown and lines are smoothed by cubic spline fits.

nss-SO$_4^{2-}$ - sea ice 60°W- 30°W (Neumayer)

Fig. 5. Magnitude squared coherence between the NM (nss-SO$_4^{2-}$)$_{anomaly}$ and the SIE at 60°W-30°W (bold black line; grey line: p = 0.05 significance level).

Fig. 6. Magnitude squared coherence between the NM $(nss\text{-}SO_4^{2-})_{anomaly}$ and local temperature T, (bold black line; grey line: $p = 0.05$ significance level).

MS – T (Neumayer)

Fig. 7. Magnitude squared coherence between the NM (MS)$_{anomaly}$ and local temperature T, (bold black line; grey line: p = 0.05 significance level).

Fig. 8. Scatter plots of annual mean ion concentrations measured at NM (abscissa) and DDU (ordinate), respectively. The regression line for NO_3^- is based on a bivariate reduced major axis (RMA) regression: $y = 0.75(\pm0.16) - 0.5(\pm6)$, $r^2 = 0.47$.

Fig. 9. Annual means of: (a) MS (grey bars) and nss-SO_4^{2-} (white bars), (b) Na^+, all at NM, (c) SIE 60°W-30°W (white bars) and SIE 30°W-30°E (grey bars).

Fig. 10. Results from Monte Carlo Singular Spectrum Analyses (MC-SSA). Plotted are the sum of corresponding reconstructed components (RCs) showing periodicities larger than one year: (a) MS (solid line) and nss-SO_4^{2-} (dashed line) anomaly reconstructions according to EOF 1+2 each. (b) SAM reconstruction according to EOF 1+2. Grey vertical bars mark El Niño events.
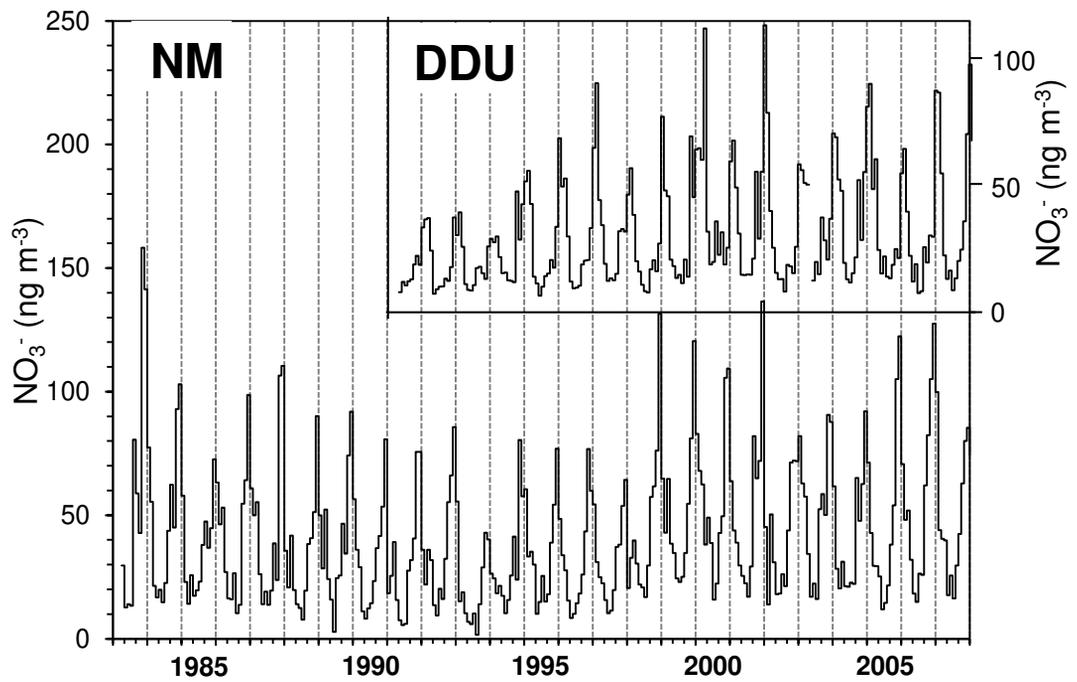
Fig. 11. Comparison of the monthly mean NO$_3^-$ record observed Neumayer (lower panel) and DDU (upper panel).

Appendix S1

Short description of the methods used for time series analyses

S.1.1. General remarks

The intention of the following sections is to show the principal approach of the applied statistical methods and why they are especially adapted for our purpose, but not to provide a complete treatise of the mathematical formalisms. Thorough descriptions of the mathematical procedures used here are available in the referenced literature. All calculations were conducted with MatLab software (The Mathworks^{TM}).

S.1.2. Mann-Kendall test with Sen's slope

First of all we have to consider the fact that none of the time series to be evaluated here were normally distributed, but have an approximate lognormal distribution. Thus we used the nonparametric rank-order Mann-Kendall test (Hirsch et al., 1982; Sirois, 1998) to verify whether a statistically significant trend (i.e. on a 95% confidence level of a two-tailed test) was present. Given so, the slope was estimated by the likewise nonparametric Sen's slope method (Sen, 1968) with a corresponding MatLab script written by Burkey (http://www.mathworks.com/matlabcentral/fileexchange/11190). Sen's slope is defined as the median of the individual slopes of all non repeating data pairs of a given time series. Both methods are especially suitable for data sets with gaps and outliers and are independent on their distribution.

S.1.3. Monte-Carlo Singular Spectrum Analysis (MC-SSA)

Singular Spectrum Analysis (SSA) is particularly suited for extracting oscillatory patterns (harmonic as well as non harmonic oscillations) from short and noisy time series (Broomhead and King, 1986; Vautard and Ghil, 1989; Ghil et al., 2002). First of all the time series of

interest was embedded into a vector space of dimension M, i.e. one constructs a sequence of M-dimensional vectors $X^*(\tau)$ from the original time series vector $X(\tau)$ as follows:

$$X^*(\tau) = \{X(\tau), X(\tau+1),\ldots, X(\tau+M-1)\}$$

with $\tau = 1,\ldots,N'$ and $N' = N-M+1$. The lag time step (in our case the sampling interval of one month) should be large enough to ensure that subsequent samples are uncorrelated, i.e. the samples have to be statistical independent. We generally used M = 60 (but also tested M = 20, 50, and 120), which emerged as a good trade-off between the quantity of information obtained (M as large as possible, but should not exceed $1/3 \cdot N$ (Vautard et al., 1992)) against the degree of statistical confidence (requiring in contrast a large N/M-ratio). With SSA harmonic or at least intermittent periods in the range between $1/5 \cdot M$ and M (i.e. in our case between 12 months and 5 years for M = 60) can be resolved (Vautard et al., 1992). In a second step the singular value decomposition of the N'xM trajectory matrix of the vectors $X^*(\tau)$ provides the square roots of the eigenvalues λ_k as well as the associated eigenvectors ρ_k, the so-called Empirical Orthogonal Functions, EOFs (Broomhead and King, 1986). The embedded time series can be projected onto a given EOF yielding the corresponding principal component (PC_k):

$$PC_k(t) = \sum_{j=1}^{M} X(t+j-1)\rho_k(j)$$

Finally, a reconstructed time series (RC_k) based on a selected EOF or a chosen combination of EOFs can be calculated according to Vautard et al., (1992):

$$RC_k(t) = \frac{1}{M_t} \sum_{k} \sum_{j=L}^{U} PC_k(t-j+1)\rho_k(j)$$

$$(M_t, L, U) = (1/t, 1, t), \qquad\qquad 1 \le t \le (M-1)$$
$$(M_t, L, U) = (1/M, 1, M), \qquad\qquad M \le t \le N'$$
$$(M_t, L, U) = (\tfrac{1}{N-t+1}, t-N+M, M), \qquad N'+1 \le t \le N$$

The adapted weighting factor M_t as well as the lower and upper boundary L and U are necessary due to the Hankel structure of the matrix constituted by the embedded time series (this procedure is also known as diagonal averaging). In short, this method generates data-adaptive filters (the EOFs) for a separation of the original time series into statistically independent compounds (the PCs) from which finally noise reduced time series can be reconstructed (the RCs) from the original record.

S.1.4. Multitaper Method (MTM)

The Multitaper Method is particularly capable in analysing time series whose spectrum potentially contain broadband (non-harmonic) as well as line (harmonic) components. Filtering or noise reduction, in our case achieved by MC-SSA, minimises the number of spurious spectral peaks (Vautard et al., 1992), which is the main drawback of MTM. MTM is non-parametric and reduces the variance of a spectral estimate by using a small set of specific tapers in contrast to common methods where a unique spectral window (e.g. peridogram and Blackman-Tukey approach) is employed. We generally used three tapers, which emerged as an appropriate trade-off between spectral resolution Δf (with $\Delta f = 0.5 \cdot (\kappa+1) \cdot f_r$, where $f_r = (2 \cdot \Delta t)^{-1}$ is the Nyquist frequency, Δt the sampling interval, and κ the number of employed tapers) against the degree of statistical confidence and small spectral leakage (requiring in contrast a large number k of tapers). The employed orthogonal tapers were constructed by solving a variational problem of minimising leakage outside a given frequency band (Thompson, 1982; Percival and Walden, 1993).

The calculation of magnitude-squared coherence (MSC) between two time series X(t) and Y(t) was also based on MTM spectral approach. For this purpose used a MatLab script by Huybers (http://www.mathworks.com/matlabcentral/fileexchange/22551). Especially for cross spectral analyses appropriate smoothing is critical. Excessive smoothing (large number of tapers) could entail serious frequency shifts of peaks in the coherency spectrum, while higher spectral resolution (less tapers) causes an overestimate of coherency (von Storch and Zwiers, 1999). Hence we generally varied the number of tapers between three and five for calculating coherency spectra. Provided that in all cases consistent and statistically significant results were obtained, the analysis was considered as meaningful. To estimate statistical significance we used here a nonparametric random phase approach according to Ebisuzaki (1997) which is more stringent for this kind of correlation analysis. To this end magnitude-squared coherence of surrogate data sets were performed, generated by corresponding 1000 Monte Carlo realizations of phase randomized records.

S.1.5. Continuous wavelet transform (CWT) and wavelet coherence transform (WCT)

In order to detect intermittent coherences (localized on the time axis) in the time frequency space, wavelet coherence was employed, based on an approach by Grinsted et al. (2004). This

method is predicated on continuous wavelet transform (Kumar and Foufoula-Georgiou, 1997). Generally by CWT, a discrete time series X(n) is convoluted with a specific window or analysing function $\Psi[(n'-n)\delta t/s]$:

$$W_\psi^X(n,s) = \sum_{n'=0}^{N-1} X(n)\Psi^*\left[\frac{(n'-n)\delta t}{s}\right]$$

$\Psi[(n'-n)\delta t/s]$ is called wavelet, a function which must have zero mean and be localized in time and frequency space. Wavelets can be n-translated across the time series to be analysed and s-dilated (Torrence and Compo, 1998). The variable s defines the wavelet scale and corresponds to the width of the analysing wavelet in the time domain, while n is the localized time index, δt the analysing time step, and (*) means the complex conjugate. For our purpose the complex Morlet wavelet was chosen, which provides a suitable trade-off between time and frequency resolution (ω_0 is a dimensionless frequency, in our case $\omega_0 = 6$; η is a dimensionless time scale):

$$\psi_0(\eta) = \pi^{-1/4}e^{i\omega_0\eta}e^{-\frac{1}{2}\eta^2}$$

In this way the time series is decomposed into a time-frequency space and both, the dominant modes of variability as well as their temporal behaviour can be determined. Finally, the wavelet coherence transform (WCT) between two data vectors $X(\tau)$ and $Y(\tau)$ is defined as:

$$R_\eta^2(s) = \frac{\left|S(s^{-1}W_\psi^X(s)W_\psi^Y(s)^*)\right|^2}{S(s^{-1}\left|W_\psi^X(s)\right|^2)\cdot S(s^{-1}\left|W_\psi^Y(s)\right|^2)}$$

Where S is a necessary smoothing operator in the time and frequency axis (Grinsted et al, 2004).

S.1.6. Statistical significance against red noise

For the spectral methods employed here (except MSC), we estimated the statistical significance against red noise, which is typical for geophysical time series. To this end we used surrogate sets of a normalised univariate autoregressive process of first order (AR(1) or Markov process):

$$x(\tau) = \alpha \cdot x(\tau-1) + z(\tau)$$

Where α is the lag-1 autocorrelation, $z(\tau)$ is a (normalised) Gaussian white noise process. The coefficients α and $z(\tau)$ were first estimated from the given time series $X(\tau)$ by using a maximum likelihood criterion. The implementation of this significance test for SSA was first described by Allen and Smith (1996) and is called Monte Carlo SSA (MC-SSA).

References

Allen, M.R. and Smith, L.A. 1996. Monte Carlo SSA: Detecting irregular oscillations in the presence of colored noise. *J. Clim.* **9**, 3373-3404.

Broomhead, D.S., and King, G.P. 1986. Extracting qualitative dynamics from experimental data. *Phys. D* **20**, 217-236.

Ebisuzaki, W. 1997. A method to estimate the statistical significance of a correlation when the data are serially correlated. *J. Clim.* **10**, 2147-2153.

Ghil, M., Allen, M.R., Dettinger, D., Die, K., Kondrashov, D., and co-authors. 2002. Advanced spectral methods for climatic time series. *Rev. Geophys.* **40**, 1-41, doi:10.1029/2001RG000092.

Grinsted, A., Moore, J.C., and Jevrejeva, S. 2004. Application of the cross wavelet transform and wavelet coherence to geophysical time series. *Nonlinear Processes in Geophysics* **11**, 561-566.

Hirsch, R.M., Slack, J.R., and Smith, R.A. 1982. Techniques of trend analysis for monthly water quality data. *Water Resour. Res.* **18**, 107-121.

Kumar, P. and Foufoula-Georgiou, E. 1997. Wavelet analysis for geophysical applications. *Rev. Geophys.* **35**, 385-412.

Percival, D.B., and Walden, A.T. 1993. *Spectral Analysis for Physical Applications.* Cambridge Univ. Press, New York, 583 pp.

Sen, P.K. 1968. Estimates of the regression coefficient based on Kendall's tau. *J. Am. Stat. Assoc.* **63**, 1379-1389.

Sirois, A. 1998. A brief and biased overview of time-series analysis of how to find that evasive trend. WMO/EMEP Workshop on advanced statistical methods and their Application to Air Quality data sets, annex E. *Global Atmos. Watch* **133**, TD-No. 956, World Meteorol. Organ., Geneva.

Thompson, D.J. 1982. Spectrum estimation and harmonic analysis. *Proc. IEEE* **70**, 1055-1096.

Torrence, C., and Compo, G.P. 1998. A practical guide to wavelet analysis. *Bull. Am. Meteorol. Soc.* **79**, 61-78.

Vautard, R. and Ghil, M. 1989. Singular spectrum analysis in nonlinear dynamics, with applications to paleoclimatic time series. *Phys. D* **35**, 395-424.

Vautard, R., Yiou, P., and Ghil, M. 1992. Singular spectrum analysis: A toolkit for short, noisy chaotic signals. *Phys. D* **58**, 95-126.

Von Storch, H. and Zwiers, F.W. 1999. In: *Statistical Analysis in Climate Research*, pp. 282-287. Cambridge University Press, Cambridge.

Appendix S2

Presentation of ancillary time series

In the following section we present time series of the ionic compounds measured at DDU (Fig. S2.1), meteorological parameters from NM (Fig. S2.2) and climate related parameters as there are SIE 60°W – 30W and SIE 30°W – 30°E, SAM and SOI (Fig. S2.3). In addition corresponding anomalies are shown, except for SAM and SOI which are anomalies per se. All data are presented in monthly binned means.
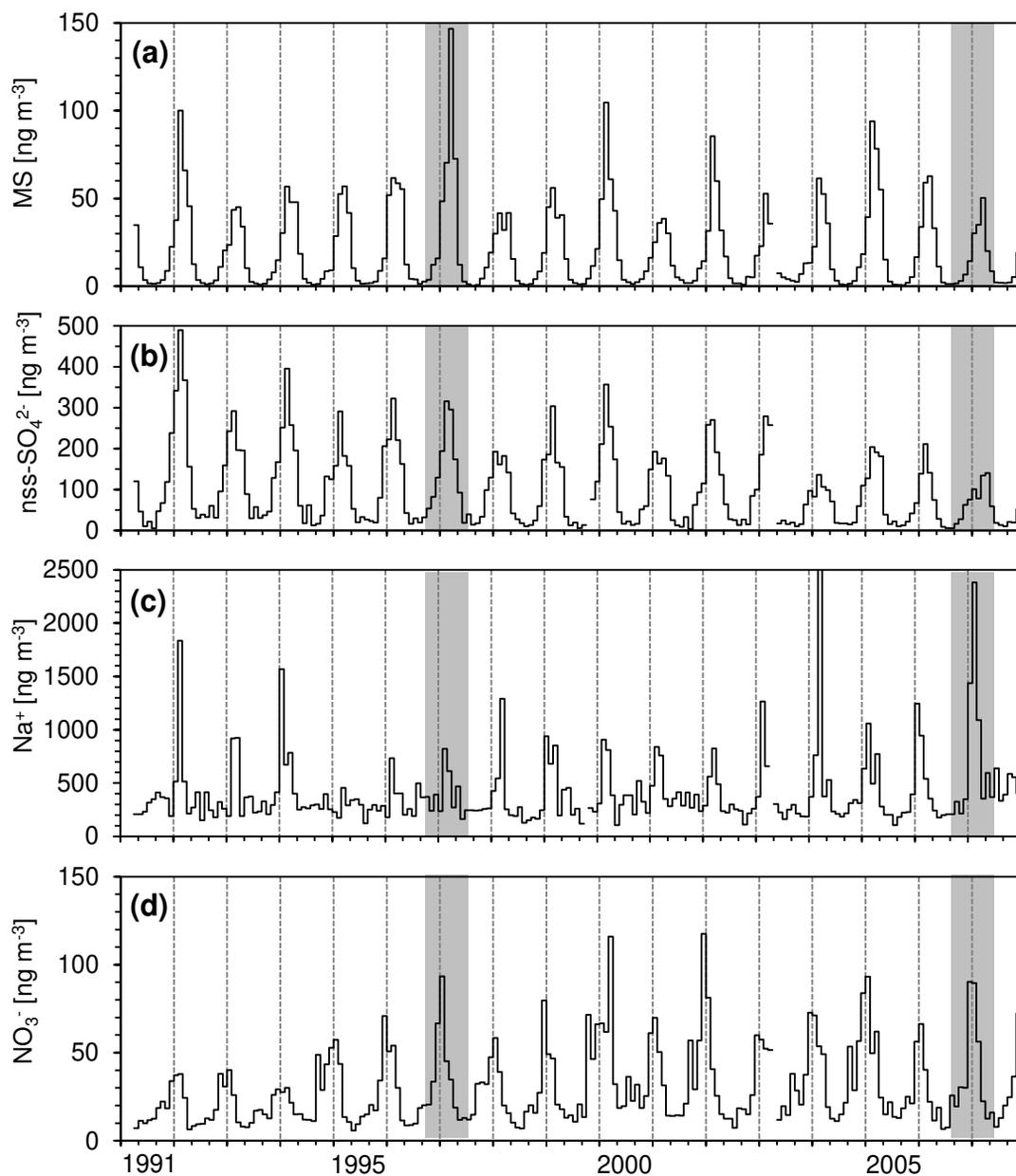
Fig. S2.1. Monthly binned mean concentrations of ionic aerosol components observed at DDU: (a) MS; (b) nss-SO_4^{2-}; (c) Na^+; (d) NO_3^-. Grey vertical bars mark distinct El Niño events (1997 and 2006).
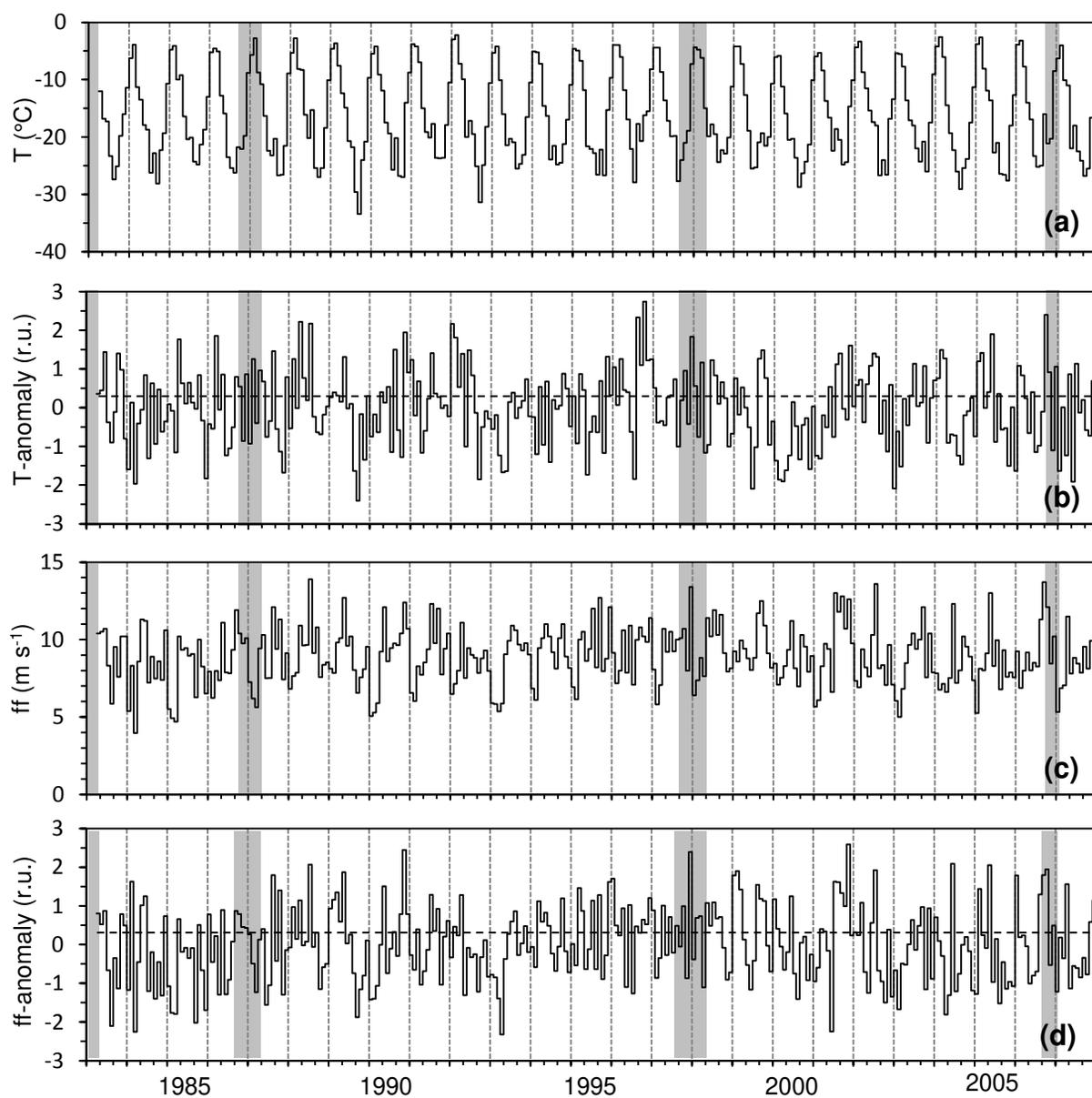
Fig. S2.2. Meteorological time series from NM: (a) Temperature; (b) temperature anomalies; (c) wind speed; (d) wind speed (ff) anaomalies (in relative units, r.u.). All data correspond to monthly binned means. Grey vertical bars mark distinct El Niño events (1982, 1986, 1997, and 2006).
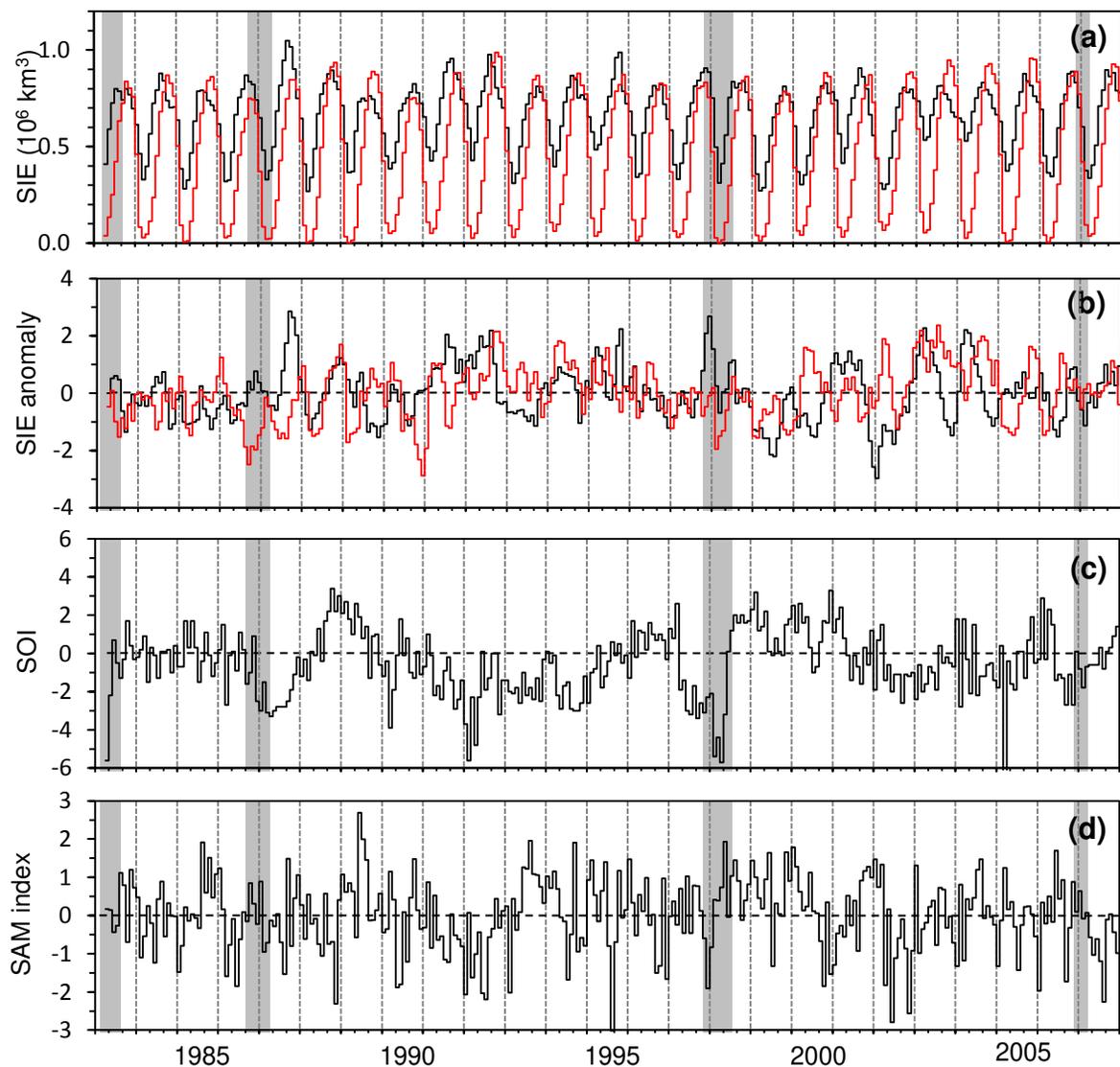
Fig. S2.3. Time series of: (a) SIE 60°W-30°W (black line) and SIE 30°W-30°E (red line); (b) anomalies of SIE 60°W-30°W (black line) and of SIE 30°W-30°E (red line); (c) Southern Ocean Index (SOI); (d) Southern Annular Mode (SAM). All data correspond to monthly binned means. Grey vertical bars mark distinct El Niño events (1982, 1986, 1997, and 2006).

Appendix S3

Ancillary results regarding spectral coherence

S.3.1. MC-SSA results

In the following section we present the results of the MC-SSA evaluation for the ionic compounds observed at NM (Fig. S3.1) and for the auxiliary data (Fig. S3.2). For SIE 30°W-30°E and SAM a clear separation of the eigenvalues of leading empirical orthogonal functions (EOFs) from the flat tail of the eigenvalue spectrum was not given (see Fig. S3.1 and S3.2, right hand part of the figures). In other words: for those records a clear separation of signal (trend and/or periodicities) from noise could not be achieved by MC-SSA. The results of the Monte Carlo red noise simulations are shown in these diagrams as dashed vertical lines representing the 95th (upper end) and 5th (lower end) percentiles of the eigenvalue distribution based on 2000 simulations. Eigenvalues from data EOFs above the respecting 95th red noise percentile correspond to a $p < 0.05$ significance level.

S.3.2. Further MSC and WCT results

Figures S3.3 through S3.6 show the results of the WCT analyses referring to the corresponding MSC results already shown in the main text (Figs. 4-7). Concerning MSC and WCT analyses based on observations at DDU, only between NO_3^- and SAM significant coherent periodicities could be detected (Fig. S3.7).
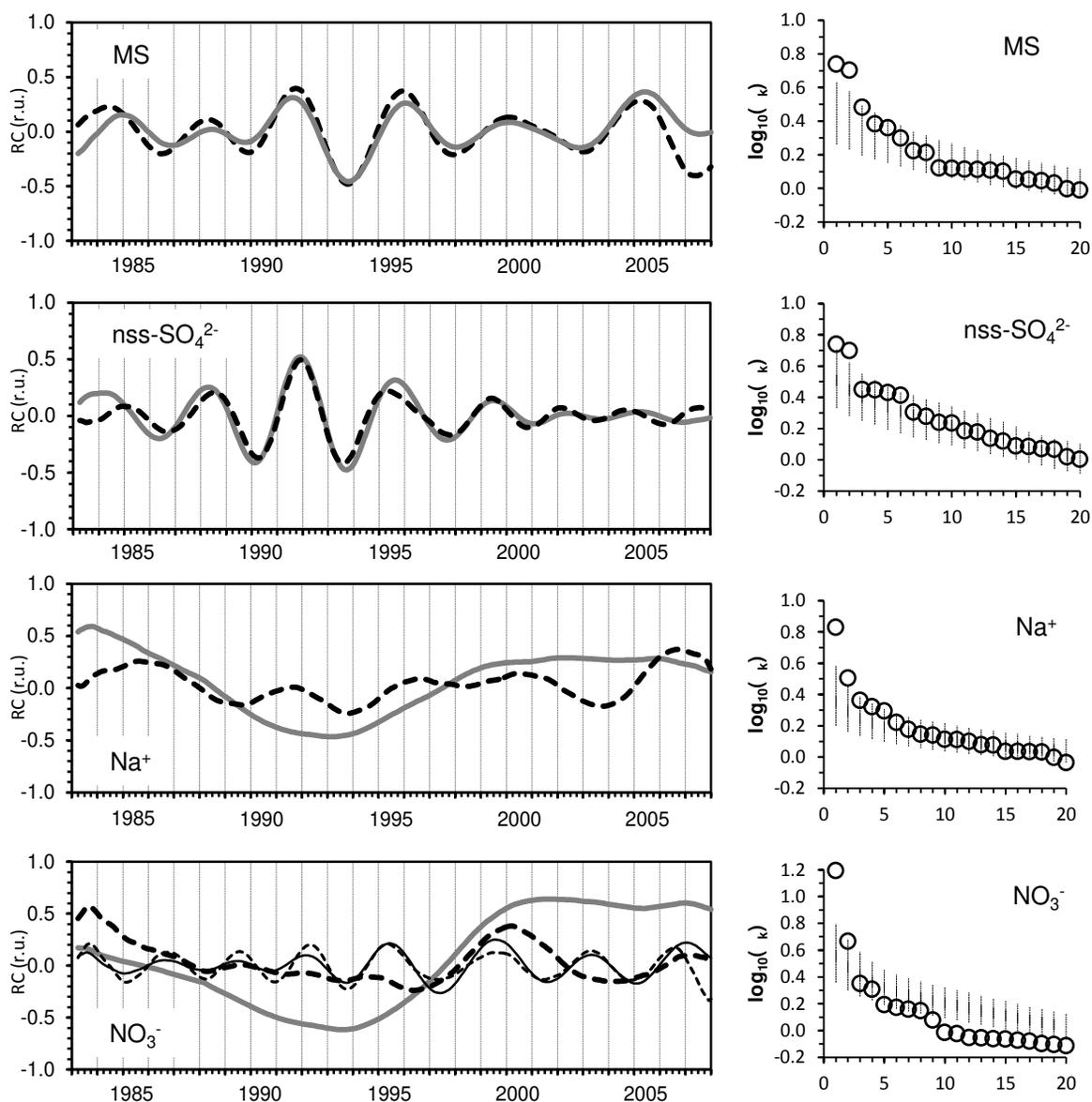
Fig. S3.1. Results from the MC-SSA analyses (embedding dimension: M = 60) for monthly anomalies of MS, nss-SO_4^{2-}, Na^+ and NO_3^- measured at NM. Left hand column: Reconstructions based on EOF 1 (bold grey line), EOF 2 (bold dashed black line), EOF 3 (thin black line), and EOF 4 (thin dashed black line). Right hand column: First 20 eigenvalues $_k$ (circles) of the corresponding EOFs, logarithmic scale. Vertical lines indicate the 95th (upper end) and 5th (lower end) red noise percentiles based on 2000 Monte Carlo simulations.
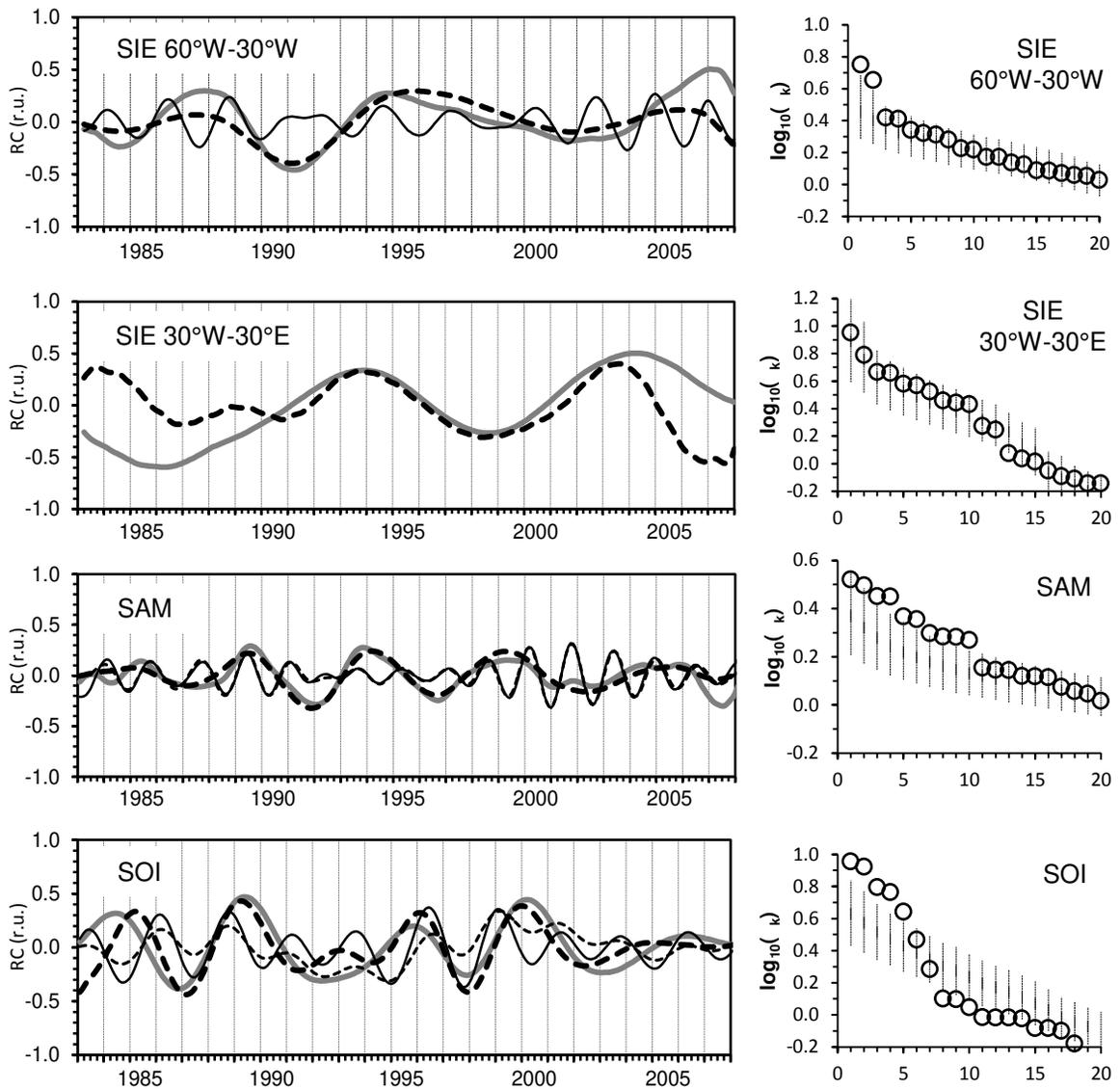
Fig. S3.2. Results from the MC-SSA analyses (embedding dimension: M = 60) for monthly anomalies of SIE, SAM, and SOI. Left hand column: Reconstructions based on EOF 1 (bold grey line), EOF 2 (bold dashed black line), EOF 3 (thin black line), and EOF 4 (thin dashed black line). Right hand column: First 20 eigenvalues $_k$ (circles) of the corresponding EOFs, logarithmic scale. Vertical lines indicate the 95th (upper end) and 5th (lower end) red noise percentiles based on 2000 Monte Carlo simulations.
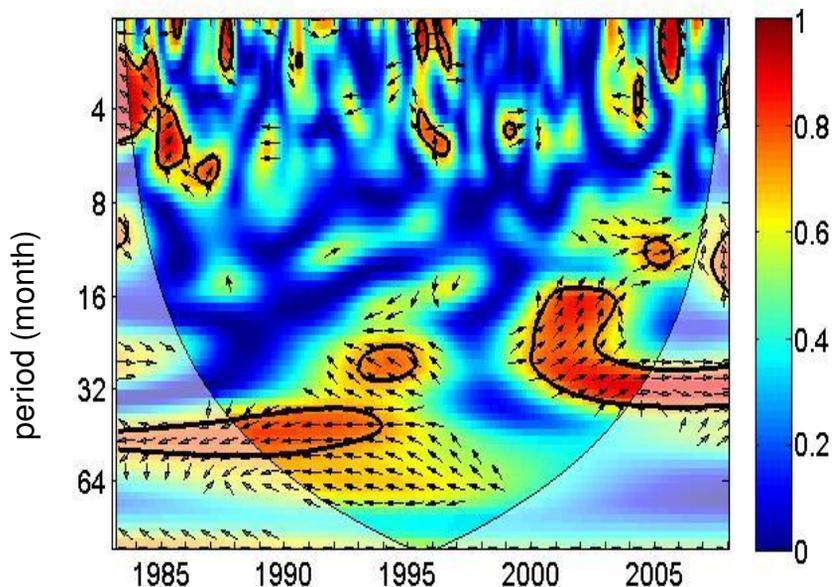
Fig. S3.3. Wavelet coherence (in colour shaded contours according to colour bar) between the time series $(nss\text{-}SO_4^{2-})_{anomaly}$ measured at NM and SAM. The bold contour lines encompass the 0.05 significance level against red noise and the cone of influence (COI) where edge effects become significant. Arrows indicate the relative phase relation (in-phase: pointing right; SAM leading ion signal by /2: pointing upright).
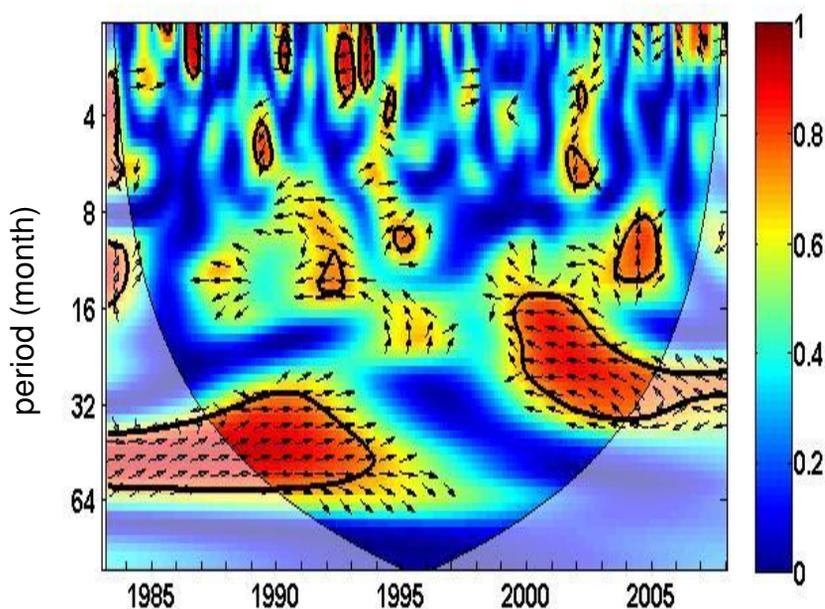

Fig. S3.4. Wavelet coherence between the time series $(nss\text{-}SO_4^{2-})_{anomaly}$ measured at NM and SIE for the region 60°W-30°W. Description see Figure S3.3.
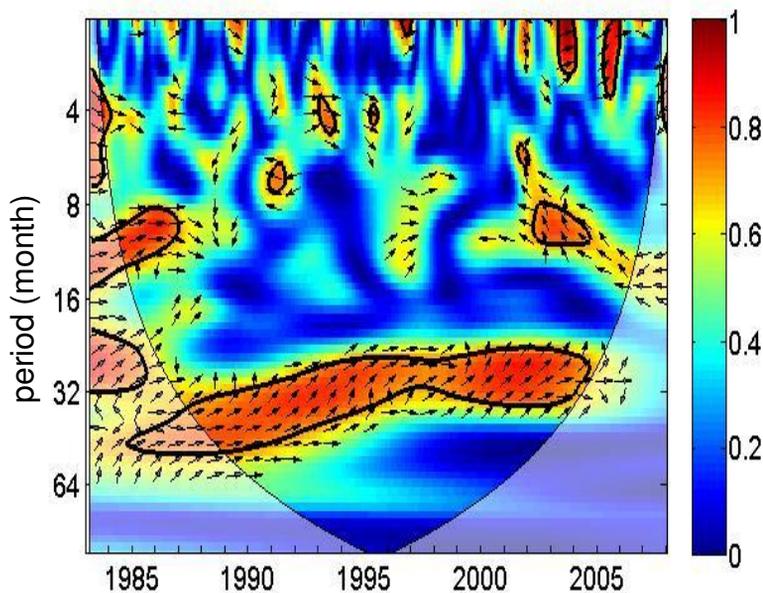
Fig. S3.5. Wavelet coherence between the time series (nss-SO$_4^{2-}$)$_{anomaly}$ and temperature at 2 m height measured at NM . Description see Figure S3.3.

.
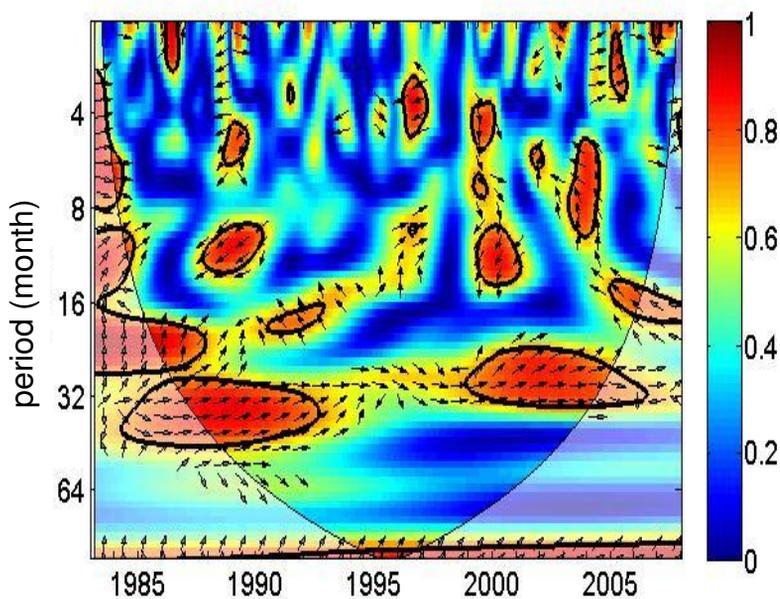
Fig. S3.6. Wavelet coherence between the time series (MS)$_{anomaly}$ and temperature at 2 m height measured at NM. Description see Figure S3.3.
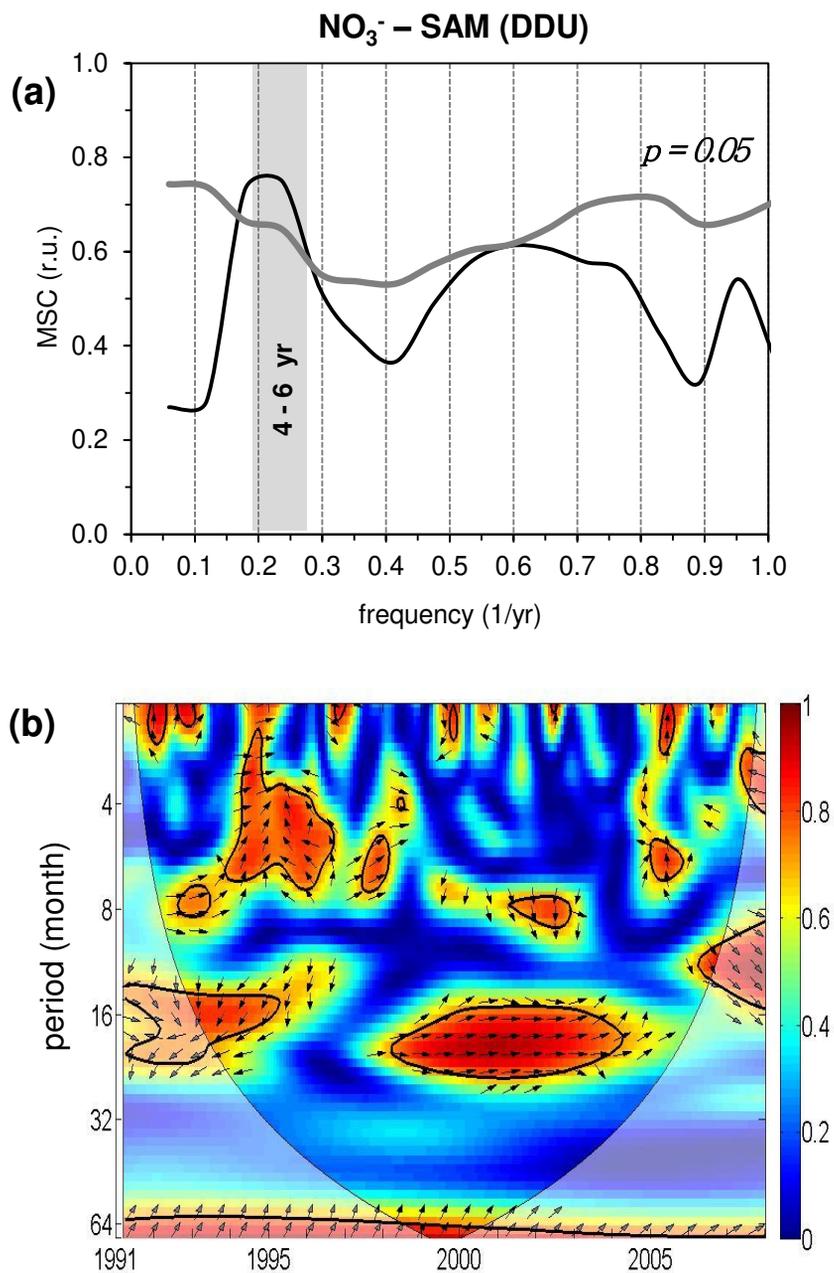
Fig. S3.7. (a) Magnitude squared coherence between $(NO_3^-)_{anomaly}$ measured at DDU and SAM. (b) Results from wavelet coherence. Description see Figure S3.3.